




## RESEARCH ARTICLE

# Estimating soil water content in a thorny forest ecosystem by time-lapse electrical resistivity tomography (ERT) and HYDRUS 2D/3D simulations

Carlos A. Faúndez Urbina<sup>1</sup>  | Daniel Cabrera Alanís<sup>2</sup> | Elizabeth Ramírez<sup>3</sup> | Oscar Seguel<sup>4</sup> | Ivo J. Fustos<sup>5</sup>  | Pablo Díaz Donoso<sup>2</sup> | Jarbas Honorio de Miranda<sup>6</sup> | Nikola Rakonjac<sup>7,8</sup> | Sebastián Elgueta Palma<sup>9,10</sup>  | Mauricio Galleguillos<sup>11,12</sup>

<sup>1</sup>Escuela de Agronomía, Facultad de Ciencias Agronómicas y de los Alimentos, Pontificia Universidad Católica de Valparaíso, San Francisco S/N, Quillota, Chile

<sup>2</sup>Departamento de Agro-Geofísica, Aquadetect, Curicó, Chile

<sup>3</sup>Facultad de Ciencias Físicas y Matemáticas, Universidad de Chile, Santiago, Chile

<sup>4</sup>Facultad de Ciencias Agronómicas, Universidad de Chile, Santiago, Chile

<sup>5</sup>Departamento de Ingeniería en Obras Civiles, Facultad de Ingeniería y Ciencias, Universidad de La Frontera, Temuco, Chile

<sup>6</sup>Departamento de Engenharia de Biosistemas (LEB), Universidade de São Paulo, Escola Superior de Agricultura "Luiz de Queiroz" (ESALQ, USP), Piracicaba, Brazil

<sup>7</sup>Soil Physics and Land Management Group, Wageningen University, Wageningen, The Netherlands

<sup>8</sup>Laboratory of Ecohydrology, École Polytechnique Fédérale de Lausanne (EPFL), Lausanne, Switzerland

<sup>9</sup>Facultad de Medicina Veterinaria y Agronomía, Universidad de las Américas, Santiago, Chile

<sup>10</sup>Núcleo en Ciencias Ambientales y Alimentarias (NCAA), Universidad de las Américas, Santiago, Chile

<sup>11</sup>Facultad de Ingeniería y Ciencias, Universidad Adolfo Ibañez, Peñalolen, Chile

<sup>12</sup>Center for Climate and Resilience Research (CR2), Universidad de Chile, Santiago, Chile

## Correspondence

Mauricio Galleguillos Torres, Facultad de Ingeniería y Ciencias, Universidad Adolfo Ibañez, Peñalolen, Chile.

Email: [m.galleguillos@uai.cl](mailto:m.galleguillos@uai.cl)

## Funding information

FONDAP-ANID, Grant/Award Number: 1522A000; FONDECYT de Iniciación, Grant/Award Number: 11230533; FONDECYT, Grant/Award Number: 1210932

## Abstract

Determination of soil volumetric water content ( $\theta$ ) in forest ecosystems is particularly challenging due to deep rooting systems and unknown soil vertical and spatial heterogeneity. This research aims to test two undisturbed methods, electrical resistivity tomography (ERT) and HYDRUS 2D/3D, for 2D  $\theta$  determination in a thorny forest ecosystem. The experiment consisted of infiltrating 10 L of water lasting 60 min. During infiltration, ERT measured apparent resistivity by time-lapse measurements, and  $\theta$  was measured with an FDR probe (EnviroSCAN) at 33, 63, 83, 97, and 163 cm depth close to the infiltration site. At the end of infiltration, a soil pit was dug, and 100 measurements of  $\theta$  were performed with a TDR in a 10 × 10 cm regular grid. Archie law transformed soil resistivity (ERT) into  $\theta$  using manual calibration, verified by an independent dataset. The 2D  $\theta$  profile obtained by ERT was qualitatively compared with the HYDRUS 2D/3D one. HYDRUS 2D/3D was parametrized with calibrated parameters obtained with HYDRUS 1D using 106 days of  $\theta$  obtained with EnviroSCAN. The results of HYDRUS 1D calibration and verification were satisfactory, with RMSE and Nash-Sutcliffe coefficients ranging from 0.021 to 0.034 cm<sup>3</sup> cm<sup>-3</sup> and 0.11 to 0.77, respectively. The forward HYDRUS 2D/3D  $\theta$  simulation disagrees with EnviroSCAN

data for 33 cm depth. However, it follows the trend with near to zero variation of water content at 63 cm depth. Water content determination by ERT was satisfactory with RMSE for calibration and verification of 0.017 and 0.021 cm<sup>3</sup> cm<sup>-3</sup>. HYDRUS 2D/3D and ERT comparisons were not equal, with a shallower wetting front by ERT and a deeper one for HYDRUS. Still, both wetting fronts agree with the wetting depth estimated by EnviroSCAN. We conclude that both methods are an alternative for  $\theta$  determination in heterogeneous and deep soils of forest ecosystems.

#### KEYWORDS

applied geophysics, HYDRUS 1D, *Vachellia caven*, water balance, water transfer models

## 1 | INTRODUCTION

Land water transfers are paramount in earth system processes since they are the basis of the hydrological cycle, coercing the interactions between the atmosphere and the critical zone (Yang et al., 2021). For instance, soil physical properties and water content directly modulate critical processes such as evapotranspiration or infiltration. Those variables are related to ecological water consumption (Tan et al., 2018) or the resilience of a catchment to support hydrological extremes such as drought and floods (Beevers et al., 2021). However, quantifying water transfers is challenging, particularly when considering the interaction between rooting systems and deep soils, a common situation in forest ecosystems (Balocchi et al., 2023). Forest lands, including thorny forests, are crucial in providing a diverse range of valuable ecosystem services (Smith-Ramírez et al., 2023), emphasizing the need to monitor and comprehend soil moisture dynamics within these ecosystems effectively.

Earth observation products provide valuable information for estimating water contents on a global scale (Han et al., 2023; Sungmin & Orth, 2021). Nonetheless, these estimates are obtained at coarse resolutions and accompanied by significant uncertainties, particularly in non-instrumented areas, which is a common occurrence in forest ecosystems (Melo et al., 2021). Water transfer models can be implemented to cope with such challenges. These models solve the mass balance in the vadose zone, enabling simulations of various water balance components, including evapotranspiration, runoff, soil moisture, and percolation (Moene & van Dam, 2013). Determining water balance in native forests has been recognized as a significant research gap by Balocchi et al. (2023). Accurately determining soil volumetric water content ( $\theta$ ) is critical. However, verifying  $\theta$  can be challenging, particularly when considering factors such as vertical and spatial heterogeneity, as well as the presence of deep soils.

To estimate  $\theta$ , instruments such as frequency domain reflectometry (FDR) are commonly used both in agriculture (Beyá-Marshall et al., 2022; Faúndez Urbina et al., 2022) and forestry ecosystems (Blume et al., 2008, 2009; Raab et al., 2015). Although FDR is valuable for water management assessment, it has limitations for forestry ecosystems where deep and heterogeneous soils and rooting systems are found. The limits are likewise related to a small sensing area around the probe (Ferré et al., 1998) and the soil disturbance produced during

installation. Consequently, some studies call for replacing the point-scale  $\theta$  estimate of FDR with two-dimensional monitoring methods (Chen et al., 2019). Therefore, non-invasive techniques such as geophysical methods (Turesson, 2006; Fustos et al., 2017) and mechanistic simulations (Šimunek et al., 2012) have gained the scientific community's interest in estimating  $\theta$ . Such techniques can complement or replace FDR in forestry ecosystems for  $\theta$  determination (Fäth et al., 2022; Rieder & Kneisel, 2023).

The soil exhibits distinctive electrical properties largely contingent on water content (Fustos et al., 2017). Previous investigations have facilitated the assessment of water content effects on the soil, enabling the generation of electrical resistivity profiles to proxy for variations in soil water content ( $\theta$ ). Of particular significance is the use of Electrical Resistivity Tomography (ERT), which offers unparalleled opportunities for analysing  $\theta$  distribution in both two and three dimensions, with a specific emphasis on vadose zone hydrology (Fustos et al., 2017; Garré et al., 2021). ERT involves the insertion of several electrodes at a spacing depending on the application into the soil, generating resistivity profiles that can be transformed into  $\theta$  (Samouëlian et al., 2005). The undisturbed method allowed a temporal measurement of the wetting front through time-lapse measurements (Zieher et al., 2017). Moreover, ERT allows for pixel sizes as small as 0.75 cm<sup>2</sup>, providing high-resolution profiles (Samouëlian et al., 2003). Previous studies have successfully employed ERT to determine  $\theta$  using various approaches, including petrophysical relations such as the Archie law (Brunet et al., 2010; Fan et al., 2015), the Waxman and Smits model (Chen et al., 2019), empirical equations based on the Waxman and Smits model (Garré et al., 2011), and statistical methods (Besson et al., 2010). Additionally, researchers have qualitatively compared soil resistivity against  $\theta$  in some studies (Krzeminska et al., 2022).

$\theta$  determination by mechanistic models has been customarily applied for decades (Eitzinger et al., 2004; Skaggs et al., 2004). Gridded physically based models have been applied in forestry ecosystems to cope with spatial heterogeneity (Schäfer et al., 2023). Point-scale simulations have been applied successfully to tropical (Casagrande et al., 2021) and temperate (Rabbal et al., 2018) forests with the HYDRUS model. HYDRUS is a software package that allows the solution of the Richards equation in one, two, or three dimensions using the pressure head ( $h$ ) as a state variable (Šimunek et al., 2016).

The  $h$  is then transformed into  $\theta$  using a soil hydraulic characteristic curve (e.g., van Genuchten (1980)). HYDRUS has also been applied to different scenarios, including irrigated agriculture (Pizarro et al., 2022), under saline conditions (Jia et al., 2023; Karandish & Šimůnek, 2019), rainfed vineyards with a water table (Galleguillos et al., 2017) demonstrating the robustness and flexibility of the method for  $\theta$  determination.

The combination of ERT and HYDRUS has been investigated in previous studies for determining saturated hydraulic conductivity (Farzamian et al., 2015b), fertigation patterns (Hardie et al., 2018), root water uptake (Peddinti et al., 2020) and ponded infiltration into water repellent sand (Ganz et al., 2014). One challenge of the ERT and HYDRUS combination is matching both geometries for quantitative and qualitative comparison, especially for automated matching of both geometries' grids, which is explicitly performed in this study. In this research, we tested the reliability of an ERT device and HYDRUS 2D/3D to reproduce  $\theta$  and the infiltration process in a native forest ecosystem. We established an infiltration experiment with continuous  $\theta$  measurements by FDR and TDR probes and soil laboratory analysis. Those measurements allowed the implementation of the HYDRUS water transfer model and ERT to reproduce  $\theta$  along a transect spatially. Therefore, this research aims to test two undisturbed methods, Electrical Resistivity Tomography (ERT) and HYDRUS 2D/3D, for 2D  $\theta$  determination in a *Vachellia caven* thorny forest.

## 2 | MATERIALS AND METHODS

### 2.1 | Study site description

The study was performed in 2021 in 'San Agustin' (−35.934725, −72.124604; 161 m.s.l.), located in the Cauquenes basin, Maule Region, Chile (Figure 1).

The soils are Alfisols classified as association Pocilla (CIREN, 1997). The climate in the Cauquenes basin is the Mediterranean, with a



**FIGURE 1** The study site. At the center (red circle) is found the EnviroSCAN, *Vachellia caven* tree, and the infiltration ring in between two electrodes. At the bottom of the picture is the Pinus plantation.

Köppen–Geiger climate classification of Csb type (Beck et al., 2018). Based on data from the Cauquenes meteorological station, the average annual rainfall between 1991 and 2020 was 632 mm, concentrated in the autumn–winter months. The maximum, average, and minimum annual average temperatures were 21.9, 14.8, and 7.7°C, respectively, and the annual mean reference evapotranspiration (ET<sub>0</sub>) was 1293 mm, with an aridity index of 0.49. The study site was a remnant of one hectare of thorny forest located inside a *Pinus radiata* plantation. According to satellite imagery and the tree size, the ecosystem comprises mainly *Vachellia caven* and other sclerophyllous species, such as the *Maytenus boaria* and *Schinus polygamus*, which are 30-years old. The trees had a mean height of 3.4 m and a density of 310 plants per hectare.

### 2.2 | Methodological framework

We proposed an original methodological framework composed of four steps. (i) Obtention of soil hydraulic parameters with HYDRUS-1D and laboratory analysis, (ii) A forced infiltration experiment including time-lapsed ERT measurements and a  $\theta$  grid measured by TDR, (iii) Parametrization of HYDRUS 2D/3D using calibrated HYDRUS 1D parameters and laboratory analysis. (iv) Qualitative comparison of  $\theta$  obtained by ERT and HYDRUS 2D/3D in the forced infiltration experiment.

A summary of the methodology is presented in Figure 2.

### 2.3 | HYDRUS model

The governing equation for variably saturated water flow in the soil is the Richards equation.

$$\frac{\partial \theta}{\partial t} = \frac{\partial}{\partial z} \left[ K_z(h) \left( \frac{\partial h}{\partial z} + 1 \right) \right] + \frac{\partial}{\partial x} \left[ K_x(h) \left( \frac{\partial h}{\partial x} \right) \right] - S, \quad (1)$$

where  $\theta$  is the soil volumetric water content ( $\text{cm}^3 \text{cm}^{-3}$ ),  $t$  is time (h),  $z$  and  $x$  are space coordinates (cm),  $K_{z,x}$  is the saturated hydraulic conductivity ( $\text{cm h}^{-1}$ ),  $h$  is pressure head (cm), and  $S$  is a sink term related to root water uptake ( $\text{h}^{-1}$ ). HYDRUS 1D is solved in the  $z$  space coordinate, whereas HYDRUS 2D/3D is solved in the  $z$  and  $x$  space coordinates. This research used HYDRUS 1D and 2D/3D at two different times.

### 2.4 | Obtention of soil hydraulic parameters with HYDRUS-1D and laboratory analysis

#### 2.4.1 | Soil hydraulic parameters, root distribution, and weather data for HYDRUS 1D

A detailed soil description was performed in a soil pit of 200 cm depth on July 22, 2019, following Schoeneberger et al. (2012) close to the EnviroSCAN. The soil had six soil horizons, generally loamy sand soils.

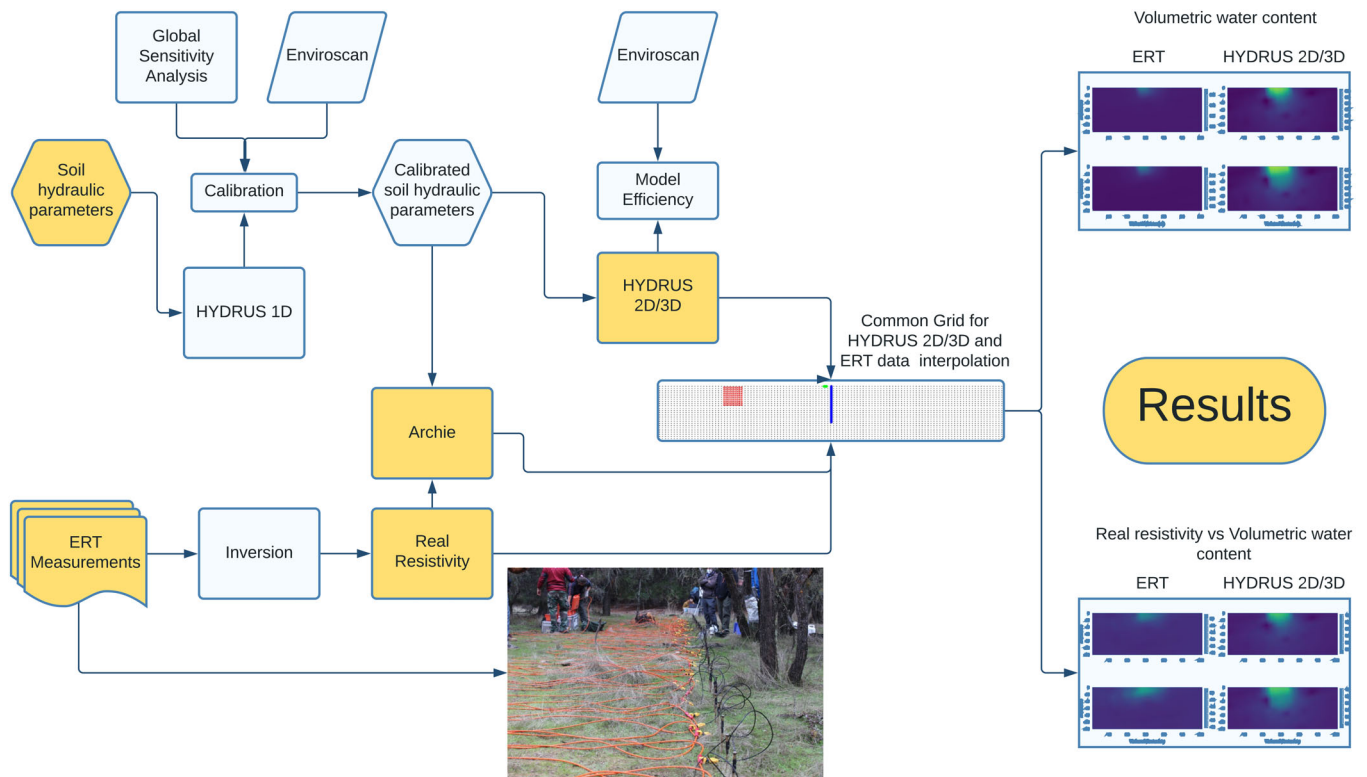


**FIGURE 2** Diagram of relevant methods and outcomes performed/obtained in this research.

Three soil samples were taken in 5 cm high and 5.9 cm diameter steel cylinders, and 1 kg of disturbed sample per each soil horizon. Those samples were analysed under laboratory conditions to obtain bulk density,  $\theta$  at field capacity and wilting point, soil texture (Bouyoucos method), and particle density (Pycnometer method) following the guidelines of Sandoval et al. (2012). Previous data was used to obtain soil hydraulic parameters (Mualem, 1976; van Genuchten, 1980) using a pedotransfer function solved by Rosetta DLL software (Schaap et al., 2001; Zhang & Schaap, 2017). The soil water retention curve obtained with Rosetta DLL was compared against additional points obtained with the soil samples at pressure:  $-0.2$ ,  $-6$ ,  $-33$ ,  $-100$  and  $-1500$  kPa. If the comparison was unsatisfactory, the soil hydraulic parameters were adjusted using the software RETc by manual calibration (van Genuchten et al., 1991) (Figure S2, Supplemental Material). The reason for not directly running RETc was because of the small amount of  $h - \theta$  data pairs.

Early results obtained with HYDRUS 1D were not satisfactory; therefore, a second field campaign was performed on September 22, 2021, to improve soil hydraulic parameters of the first three soil horizons. Three soil cylinders were taken per soil horizon (nine total) and analysed in a pressure plate apparatus at pressures 0,  $-6$ ,  $-10$ ,  $-30$ ,  $-330$ ,  $-1000$ ,  $-5000$  and  $-15\ 000$  hPa to perform a detailed soil characteristic curve with RETc. In addition, the saturated volumetric water content ( $\theta_s$ ) was updated from the fourth to sixth horizons regarding EnviroSCAN measurements during winter when groundwater rises (data not shown). The van Genuchten-Mualem parameters after previous laboratory analysis are depicted in Table 1.

The root depth and root distribution were defined, given the soil description. Fine, medium, and thick root density was assigned qualitatively in the soil pit following the guidelines of Schoeneberger et al. (2012) (Table S2, Supplemental Material). That information was used to obtain the root density at each soil horizon for simulations with HYDRUS 1D.

Meteorological data were obtained from a weather station located 15 km away from the study site at the 'Instituto de Investigaciones Agropecuarias (INIA)' of Cauquenes ( $-35\ 956\ 111$ ,  $-72\ 289\ 999$ ; 162 m.s.l.). Rainfall and ETo estimated with Penman-Monteith (Smith et al., 1990) were retrieved hourly from the weather station and set up in HYDRUS 1D.

#### 2.4.2 | HYDRUS 1D setup

HYDRUS 1D simulation was performed for soil water flow and root water uptake in one shrub tree (*V. caven*). Simulation time was hourly from 1 February 2021 until 17 May 2021, covering 106 days.

The model had six soil materials (Table 1). The depth of the soil profile was 300 cm; thus, the last soil material was enlarged to 300 cm. The soil material depth and hydraulic parameters were initially set in the model from laboratory measurements (Table 1). The initial condition (01 February 2021) was set as pressure head ( $h$ ) using  $\theta$  of FDR and the soil hydraulic characteristic curve. The hydraulic model was van Genuchten-Mualem without hysteresis (Mualem, 1976; van Genuchten, 1980).

**TABLE 1** Soil water retention curve parameters from van Genuchten–Mualem obtained at laboratory conditions and Archie law models for each soil horizon (L).

L	Depth cm	$\theta_r$ $\text{cm}^3 \text{cm}^{-3}$	$\theta_s$ $\text{cm}^3 \text{cm}^{-3}$	$\alpha$ $\text{cm}^{-1}$	$n$ –	$K_s$ $\text{cm h}^{-1}$	$m_c$ (–)	$n_a$ (–)
1	0–5	0.044	0.466	0.090	1.40	12.82	1.86	1.44 <sup>a</sup>
2	5–12	0.033	0.402	0.060	1.57	8.90	1.86 <sup>a</sup>	1.44 <sup>a</sup>
3	12–38	0.019	0.381	0.075	1.35*	7.30	1.34 <sup>a</sup>	1.7 <sup>a</sup>
4	38–90	0.031	0.295	0.056	1.56*	6.20	1.87 <sup>a</sup>	2.2 <sup>a</sup>
5	90–110	0.030	0.300	0.058	1.68	9.40	1.87 <sup>a</sup>	1.78 <sup>a</sup>
6	110–200	0.026	0.253 <sup>a</sup>	0.056*	1.54*	8.10	1.77	2.35 <sup>a</sup>

Note:  $\theta_r$  the residual water content ( $\text{cm}^3 \text{cm}^{-3}$ ),  $\theta_s$  is the saturated volumetric water content ( $\text{cm}^3 \text{cm}^{-3}$ ),  $\alpha$  ( $\text{cm}^{-1}$ ), and  $n$  (–) are empirical parameters,  $K_s$  ( $\text{cm h}^{-1}$ ) is the saturated hydraulic conductivity,  $m_c$  (–) is the cementation factor, and  $n_a$  (–) is the saturation index.

<sup>a</sup>Candidate parameter for calibration.

The top boundary condition was ‘Atmospheric with surface runoff’, which includes transpiration, evaporation, and runoff. The decision not to use a surface layer was the comparison of saturated hydraulic conductivity ( $K_s$ , Table 1) and the maximum precipitation rate equal to  $0.51 \text{ cm h}^{-1}$ . The bottom boundary was constant head because a groundwater table was simulated with the phreatic level at 240 cm depth.

Hourly precipitation and ETo are inputs for the model obtained from the weather station in Cauquenes. The HYDRUS module ‘Meteorological parameters and conditions’ split evaporation from transpiration. In that module, meteorological data obtained from the Cauquenes station, such as solar radiation, temperature, humidity, and wind, were set hourly for 106 days. Additionally, the model requires the leaf area index (LAI) and the extinction coefficient ( $k$ ). Both parameters were obtained at field conditions with CI-110 Plant Canopy Imager (Bio-Science), obtaining  $LAI = 1.5$ ,  $k = 0.55$ . The sampling was performed in three positions around the *V. caven* tree. Those parameters were set constant during the 106 days of simulation. The rainfall interception by the plant canopy was obtained using a HYDRUS module, which used previously obtained LAI, and the ‘interception parameter’ equalled  $0.25 \text{ mm d}^{-1}$ .

Roots were set per soil material (Table S2, Supplemental Material). The root water uptake was simulated in HYDRUS 1D with the S-shaped function. The S-shaped parameters, ‘pressure head in the soil that root water uptake is reduced by 50%’ ( $h_{50}$ ), and  $p$  exponent were obtained from Grinevskii (2011), giving  $h_{50} = -3330 \text{ cm}$  and  $p = 2$  for the *V. caven* tree.

### 2.4.3 | Sensitivity analysis and calibration of HYDRUS 1D parameters

Soil hydraulic parameters of Table 1 were improved by calibration comparing the  $\theta$  obtained by an FDR probe (EnviroSCAN, SENTEK, Australia) at depths 33, 63, 83, 97, and 163 cm and the  $\theta$  simulated by HYDRUS 1D at the same depths. The FDR data selected for calibration start from 01 March 2021 until 17 May 2021, covering 75 days, with recordings every 1 h. The reason for not selecting data from 01 February 2021 (starting of simulations) is related to the effect of the initial condition on HYDRUS 1D simulations.

EnviroSCAN data was calibrated using three soil samples taken at the  $\theta$  measurement depths with steel cylinders at three different times. From the samples, gravimetric water content, bulk density, and  $\theta$  were measured under laboratory conditions (Sandoval et al., 2012). The  $\theta$  obtained by EnviroSCAN were compared with the  $\theta$  under laboratory conditions with regression analysis (see Figure S1, Supplemental material). The calibrated  $\theta$  of EnviroSCAN was used for calibration.

The candidates’ HYDRUS 1D parameters for calibration were selected using a Morris Elementary Effect Screening Method (Morris, 1991). Morris’s elementary effect parameters are the number of trajectories ( $r$ ), the number of HYDRUS 1D parameters ( $k$ ), the number of levels ( $p$ ), and the grid jump ( $\omega$ ) (Pujol et al., 2021). Those parameters were set after the guidelines of Faúndez Urbina et al. (2020) as follows:  $r = 100$ ,  $k = 24$ ,  $p = 6$ , and  $\omega = 3$ . The minimum and maximum values for HYDRUS 1D parameters are shown in Table S1 (Supplemental Material). The HYDRUS 1D output analysed was the hourly  $\theta$  at the measurement depths of EnviroSCAN (33, 63, 83, 97, and 163 cm depth). The sensitivity indexes obtained from Morris’s method are the modified overall effect ( $\mu^*$ ) introduced by Campolongo et al. (2007) and the interaction between parameters ( $\sigma$ ) which were obtained with the R package ‘Sensitivity’ (Pujol et al., 2021). The  $\mu^*$  and  $\sigma$  were obtained hourly; however, they were averaged over the period to compute parameter importance. The parameter importance was evaluated following the procedures in Lammoglia et al. (2017). They defined highly influential parameters if  $\mu^* > 0.5 \mu_{\text{max}}^*$  where  $\mu_{\text{max}}^*$  is the maximum  $\mu^*$  of all the HYDRUS 1D parameters analysed. The highly influential parameters are subject to calibration.

Calibration was performed with the Model-independent Parameter Estimation & Uncertainty Analysis (PEST) package (Doherty, 2015). The observed data corresponded to the hourly EnviroSCAN measurements of  $\theta$  at 33, 63, 83, 97, and 163 cm depth, whereas the simulated data corresponded to HYDRUS 1D simulations at the same depths and times (75 days). PEST was used in ‘estimation mode,’ minimizing the objective function by a Gauss-Marquardt–Levenberg method. The observed data were divided into five observation data groups (each  $\theta$  depth) to compute the weights. The Nash–Sutcliffe model efficiency coefficient (Nash) and root mean square error (RMSE) were calculated per each observation data group (see equations in Faúndez Urbina et al. (2022); Faúndez Urbina et al. (2021)).

## 2.5 | Forced infiltration experiment and time-lapsed ERT

A forced infiltration experiment and electrical resistivity tomography (ERT) survey were performed on 18 May 2021. Ten litres of water were infiltrated inside a ring of 14.4 cm diameter in 1 h. The infiltration ring was inserted 30 cm away from the EnviroSCAN. The elapsed time of EnviroSCAN was modified from 1 hour to 1 minute. At the end of the experiment (last measurement with ERT), 100 measurements of  $\theta$  were performed with a TDR (FieldScout TDR 150, Spectrum Technologies, Inc., Illinois, USA) in a regular grid of  $10 \times 10$  cm (TDR Grid in Figure 3) located 5 m away from the EnviroSCAN.

To understand changes in the soil water content using the soil resistivity at different depths as a proxy, a multitemporal ERT survey was carried out centered in the EnviroSCAN position during the forced infiltration experiment. Geologically, the study area corresponds to a non-deformed sedimentary environment, with homogeneous features allowing half-space supposition. We generated an inversion of the resistivity model from apparent resistivity estimates. The apparent resistivity was estimated using an ERT model WDJ-4 (Chongqing Gold Mechanical & Electrical Equipment Co., China). Sixty stainless steel electrodes were inserted five centimetres into the soil, separated 0.3 m between them, obtaining a  $17.7 \times 3$  m profile.

Two measurements with ERT were done a few minutes before infiltration (Time-lapse 1), and two were performed 34 (Time-lapse 2) and 62 min (Time-lapse 3) after infiltration onset. The acquisition time of ERT lasted 28 min. The 2D inverted resistivity model was estimated using RES2DINV version 4.01 (Loke, 2001). We meshed the model considering a discretization equal to the distance between electrodes and variable high with depth. The first layer was established to 0.519 times the distance between electrodes, increasing a ratio of 1.1 in

depth. These cells are extended until the depth is defined by the apparent resistivity (3 m) using blocky least-squares inversion to minimize the difference between observed and simulated resistivity following Loke (2001). A joint inversion was performed using one ERT measurement before and two ERT measurements after infiltration. A damping factor of five was used for inversion to obtain a model with smooth variations. The normalized root means square error (NRMSE) obtained for joint inversion was 3.1%.

The soil resistivity is mathematically related to the effective saturation ( $S_e$ ) by Archie law (Samouëlian et al., 2005), as follows:

$$S_e^{n_a} = \frac{a\rho_w}{\emptyset^{m_c}\rho} + \rho_{\text{surface}}, \quad (2)$$

where  $n_a$  is the saturation index,  $a$  and  $m_c$  are constant related to the coefficient of saturation and the cementation factor, respectively. In addition,  $\rho$  and  $\rho_w$  are related to the resistivity of the formation (resistivity estimated after inversion of ERT data) and the resistivity of the pore water, respectively.  $\emptyset$  is the soil porosity,  $\rho_{\text{surface}}$  is the surface conductivity only used for heavy clay soils (Revil & Glover, 1998).

The parameter  $a$  was set as 1 (–) in Equation (2) (Glover, 2016),  $\rho_w$  was set as  $12 \Omega \cdot m$ ,  $\emptyset$  was set equal to  $\theta_s$  in Table 1 (updating calibrated ones).  $m_c$  can be estimated at fully saturated conditions because  $S_e = 1$  and the value of  $n_a$  is irrelevant; that procedure was used to estimate  $m_c$  in the first, second, and sixth soil horizons (Table 1). For the first and second horizons, the inverted resistivity data of Time-Lapse 3 was used because it was assumed that soil layers 1 and 2 were fully saturated after the forced infiltration experiment. The sixth soil layer was assumed to be fully saturated because of the phreatic table at 240 cm depth. The  $m_c$  of the remainder soil layers and  $n_a$  of all soil layers were subject to manual calibration

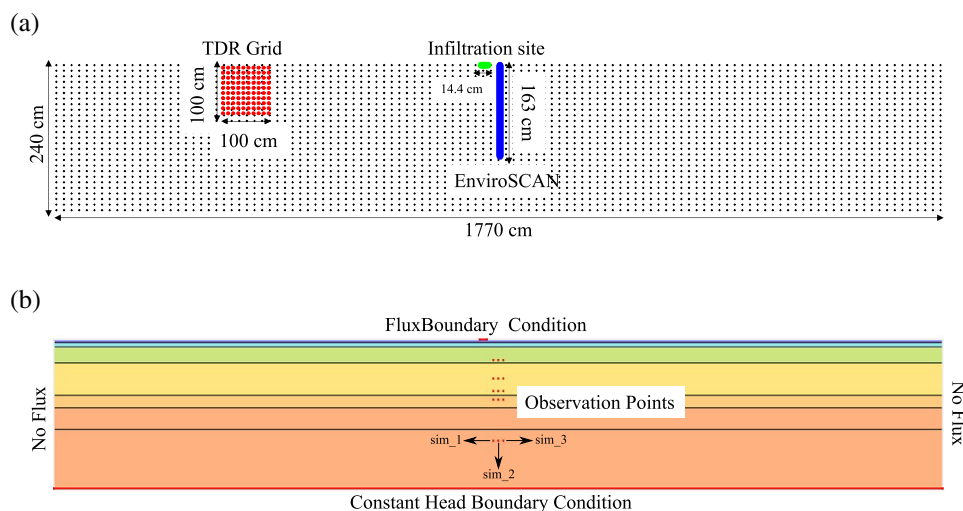


**FIGURE 3** The soil profile for ERT measurements is represented in (a). The y-axis is soil depth, and the x-axis is horizontal distance. The TDR grid corresponded to measurements performed with a portable TDR in a  $10 \times 10$  cm grid (100 points). This grid was used for calibration/verification of the Archie equation. In (b) HYDRUS 2D/3D representation of the soil profile showing boundary conditions ('flux' for infiltration and 'constant head' for the phreatic table). The observation points represent the EnviroSCAN measurement sites where sim\_1, sim\_2, and sim\_3 are observation points 20, 30, and 40 cm away from the infiltration site center.

comparing the observed (EnviroSCAN and TDR) and simulated  $\theta$  (Archie law).

For calibration of Archie's parameters, the observed  $\theta$  corresponded to 30 points from the TDR grid obtained from depths 10, 20 and 30 cm, along with  $\theta$  estimated by EnviroSCAN at Time-Lapse 1, 2 and 3. Infiltration water only modifies  $\theta$  at 33 cm EnviroSCAN depth; thus, seven observed points were obtained with EnviroSCAN data. As a result, 37 pairs of observed and simulated  $S_e$  were used for calibration. The remaining 70 points of the TDR grid (See Figure 3) were used from depths 40–100 cm to verify calibration (verification process). The root means squared error (RMSE) and normalized root mean squared error (NRMSE) were used to test calibration and verification. Additionally, Archie's subtraction of  $\theta$  and the estimated one by ERT is shown graphically.

## 2.6 | Parametrization of HYDRUS 2D/3D using calibrated HYDRUS 1D parameters and laboratory analysis

A two-dimensional domain, where water flow was simulated, was set in HYDRUS 2D/3D to match the soil profile measured by ERT after the forced infiltration experiment (Figure 3). The spatial dimension was in centimetres and time in minutes. The total simulated time was 137 min, where infiltration starts at 63 min and ends at 122 min. Therefore, 60 min in total with a rate of  $1.02 \text{ cm min}^{-1}$ . For that period, no root water uptake was considered. Six soil materials were set up in the model corresponding to the six soil horizons described in the pit. The van Genuchten-Mualem model was used with parameters obtained by calibration with HYDRUS 1D and laboratory measurements. Therefore, a forward simulation (no calibration) was performed with HYDRUS 2D/3D for  $\theta$ .

The initial conditions were set from EnviroSCAN data before infiltration (transformed to pressure head). Boundary conditions are found in Figure 3. The boundary at the infiltration site was set as flux, and the remaining top boundary conditions were set as no flux. The bottom boundary was a constant head representing the groundwater table at 240 cm. The sides of the domain were set with no flux boundary conditions. The  $\theta$  simulated by HYDRUS 2D was compared against the  $\theta$  of EnviroSCAN to test the forward simulation. For this comparison, three observation points were included in HYDRUS 2D/3D (sim\_1, sim\_2 and sim\_3 in Figure 3). The reason is related to the area measured by EnviroSCAN, which corresponds to 5 cm of radius from the probe.

## 2.7 | Comparison of $\theta$ obtained by ERT and HYDRUS 2D/3D in the forced infiltration experiment

The  $\theta$  simulated by HYDRUS 2D/3D were compared with the  $\theta$  estimated by the ERT graphically using 2D images. The images were generated from a common grid generated in Rscript. The grid was

generated in the x-axis starting at position 7 cm every 15 cm until 1740 cm, whereas, in the z-axis, it started at  $-5 \text{ cm}$  every  $-11 \text{ cm}$  until  $-280 \text{ cm}$ . ERT and HYDRUS 2D/3D  $\theta$  data were interpolated in this grid using inverse distance weighted interpolation by R package gstat (Pebesma et al., 2004). The binary data of HYDRUS 2D/3D was used to build the 2D  $\theta$  image with Rscript.

## 3 | RESULTS

### 3.1 | Sensitivity analysis and calibration of HYDRUS 1D

Figure 4 shows the highly influential parameters obtained from the Morris Elementary Effect sensitivity analysis.

The highly influential soil hydraulic parameters for  $\theta$  simulated by HYDRUS 1D at depths 33, 63, 83, 97 and 163 cm were  $n_3$ ,  $n_4$ ,  $n_6$ ,  $\alpha_6$  and  $\theta_{s6}$ . The subscript corresponds to the number of soil materials; thus,  $n_3$  is the  $n$  parameter for the third soil material and similarly for the other soil hydraulic parameters. The highly influential soil hydraulic parameters were subject to calibration. Calibrated parameters and 95% confidence limits are found in Table 2.

Table 2 shows that the calibrated soil hydraulic parameters had narrow 95% confidence limits, indicating a good calibration by the PEST model. Furthermore, comparing Table 1 with Table 2, calibrated values are close to those measured at laboratory conditions except for  $n_3$ .

Figure 5 depicts the comparison of  $\theta$  estimated by EnviroSCAN, the  $\theta$  simulated with soil hydraulic parameters obtained at laboratory conditions (forward simulation with HYDRUS 1D, Table 1), and  $\theta$  simulated by HYDRUS 1D after calibration of highly influential parameters at each depth (Tables 1 and 2).

Calibrated soil hydraulic parameters improved HYDRUS 1D simulations in all depths regarding laboratory measurements (Figure 5). The Nash is positive for all depths; however, for 33, 97 and 163 cm depth, the value was lower than 0.28. The maximum RMSE was found for 97 cm depth equals  $0.034 \text{ cm}^3 \text{ cm}^{-3}$ . The water peak after rainfall was partially matched for the first three depths (Figure 5a–c). However, the peak after rainfall was not matched for lower depths (Figure 5d,e).

### 3.2 | HYDRUS 2D/3D simulation

HYDRUS 2D/3D forward simulation using soil hydraulic parameters of Tables 1 and 2 was compared against EnviroSCAN data (Figure 6).

The comparison of HYDRUS 2D/3D against EnviroSCAN data was unsatisfactory for 33 cm depth and satisfactory for 63 cm depth. Deeper layers are not shown because the water did not reach those positions during the forced infiltration experiment. After all, just 10 L of water were infiltrated. No water content change is observed at position 63 cm of EnviroSCAN (Figure 6b), where a horizontal line is observed during time. Additionally, the  $\theta$  obtained for the three

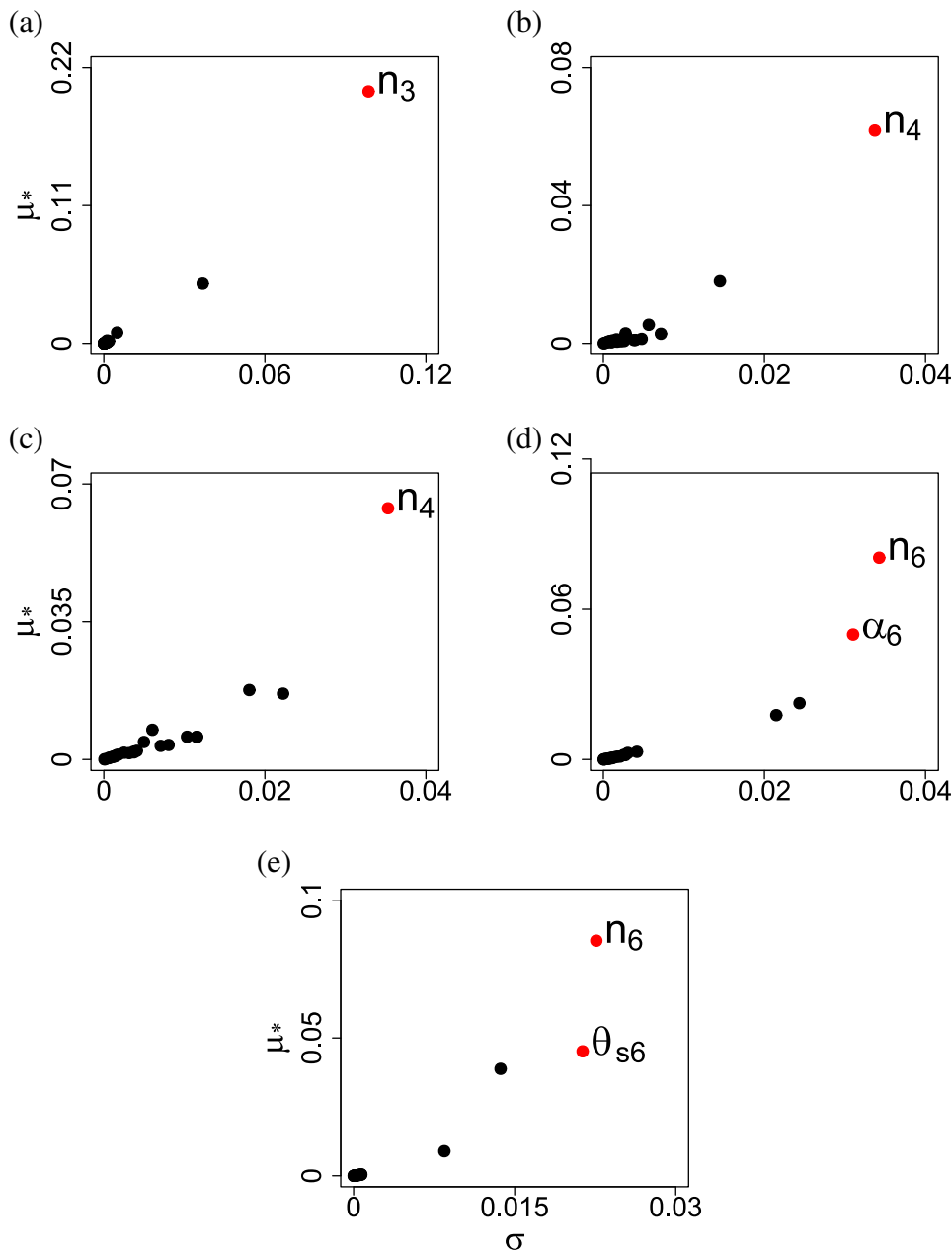


**FIGURE 4** Morris elementary effect screening sensitivity analysis method for HYDRUS 1D analysing volumetric water content ( $\theta$ ) output of the model at 33 (a), 63 (b), 83 (c), 97 (d) and 163 (e) cm depth which aligns with EnviroSCAN measurements. Red dots are highly influential parameters  $\mu^* > 0.5 \mu_{\max}^*$  whereas black dots represent the remainder of the parameters.  $n_{3,4,6}$  are the pore connectivity parameters of materials 3, 4 and 6, respectively,  $\alpha_6$  is the air entry value of material 6, and  $\theta_{s6}$  is the saturated water content of material 6. The y-axis  $\mu_i^*$  is the modified overall effect introduced by Campolongo et al. (2007), and the x-axis  $\sigma$  is the standard deviation representing the interaction between parameters.

**TABLE 2** Highly influential calibrated soil hydraulic parameters and their 95% confidence limits.

Parameter	Estimated value	95% lower limit	95% upper limit
$n_3$	2.700	2.623	2.780
$n_4$	1.392	1.386	1.398
$\theta_{s6}$	0.200	0.193	0.207
$\alpha_6$	0.047	0.046	0.048
$n_6$	1.528	1.494	1.561

Note: The subscript corresponded to the number of soil materials.  $\theta_s$  is the saturated volumetric water content ( $\text{cm}^3 \text{cm}^{-3}$ ),  $\alpha$  ( $\text{cm}^{-1}$ ), and  $n$  (–) are empirical parameters.

observation points separated 10 cm along the x-axis was highly variable (sim\_1, sim\_2 and sim\_3). This forward simulation was used for comparison against ERT  $\theta$  estimations graphically.

### 3.3 | Water content determination by ERT

The  $\theta$  obtained by ERT using the inverted resistivity and the Archie equation (Equation (2)) is depicted in Figure 7 for time-lapsed 1 (before infiltration) and time-lapsed 2 (34 min after infiltration) and time-lapsed 3 (62 min after infiltration).

The infiltrated water is visible over time (Figure 7b,c). Calibrated Archie parameters ( $m_c$  and  $n_a$ ) are found in Table 1. Calibration and verification of the  $\theta$  using the Archie equation are depicted in Figure 8.

The  $\Delta\theta$  was obtained by subtracting the  $\theta$  obtained by the TDR grid (Figure 3) against  $\theta$  obtained by Archie. It is observed overestimation (reddish colours) and underestimation (bluish colours) by Archie in  $\theta$  values (Figure 8). The RMSE obtained for the calibration of Archie (using 37 points) was  $0.017 \text{ cm}^3 \text{cm}^{-3}$ , whereas the RMSE for verification (70 points) was  $0.021 \text{ cm}^3 \text{cm}^{-3}$ . The NRMSE for calibration and verification was 16.4% and 18.9%, respectively.



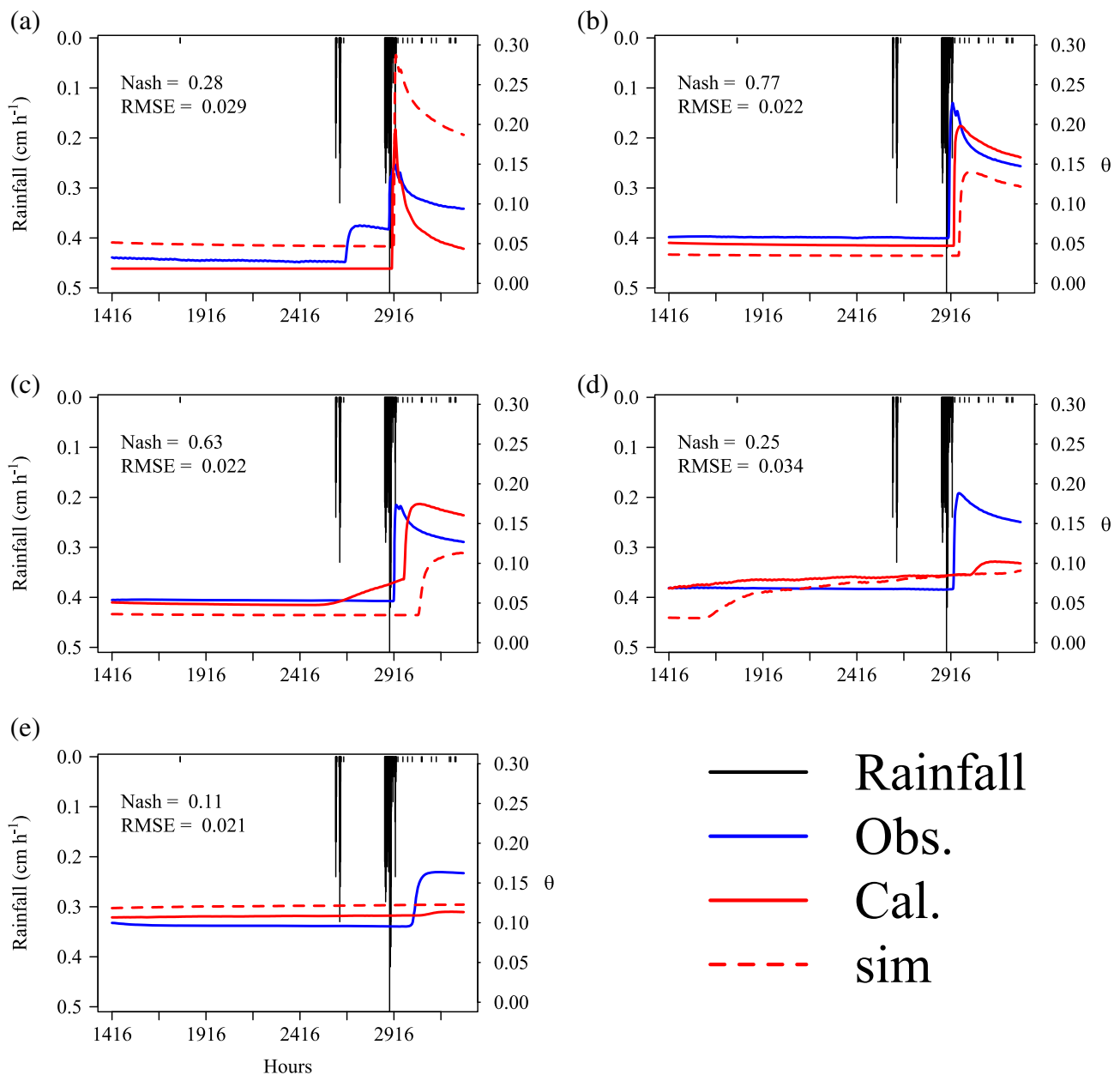


**FIGURE 5** Volumetric water content ( $\theta$ ,  $\text{cm}^3 \text{cm}^{-3}$ ) measured by EnviroSCAN ('Obs.' continuous blue line) and simulated by HYDRUS 1D with ('Cal.' Continuous red line) and without ('sim' dashed red line) calibration of van Genuchten–Mualem parameters at 33 (a), 63 (b), 83 (c), 97 (d), and 163 (e) cm depth. The left y-axis represents rainfall (continuous black line,  $\text{cm h}^{-1}$ ), the right y-axis represents  $\theta$ , and the x-axis represents the time in hours (Julian) where 1416 = 01 March 2021 00:00:00. The Nash-Sutcliffe coefficient (Nash, unitless) and the root mean square error (RMSE,  $\text{cm}^3 \text{cm}^{-3}$ ) are depicted only after calibration.

### 3.4 | Comparison of HYDRUS 2D/3D and ERT

The comparison of the change of volumetric water content ( $\Delta\theta$ ,  $\text{cm}^3 \text{cm}^{-3}$ ) obtained by ERT using calibrated Archie values and HYDRUS 2D/3D using calibrated parameters of HYDRUS 1D is depicted in Figure 9. Note that the image is a zoom of Figure 7 for highlighting the infiltration zone and wetting front.

The comparison between ERT and HYDRUS 2D/3D depicts that the water infiltrated into the soil generated by ERT produces a shallower wetting front than the one generated with HYDRUS. To verify if this difference was produced for the transformation of inverted

resistivity data into  $\theta$  by Archie law, a comparison of the change of inverted resistivity data by ERT and the change of  $\theta$  ( $\Delta\theta$ ,  $\text{cm}^3 \text{cm}^{-3}$ ) obtained by HYDRUS 2D/3D is depicted in Figure 10. The change of inverted resistivity ( $\Delta\rho_{(\log)}, \Omega \cdot m$ ) data was transformed to obtain a comparable colour scale with HYDRUS 2D/3D.

It is observed in Figure 10 that the comparison of inverted resistivity data ( $\Delta\rho_{(\log)}, \Omega \cdot m$ ) by ERT and change of  $\theta$  ( $\Delta\theta$ ,  $\text{cm}^3 \text{cm}^{-3}$ ) by HYDRUS 2D/3D improve concerning the one obtained in Figure 9. The wetting front of ERT is slightly more profound than the previously obtained. However, it still is not the same as the one obtained by HYDRUS 2D/3D.

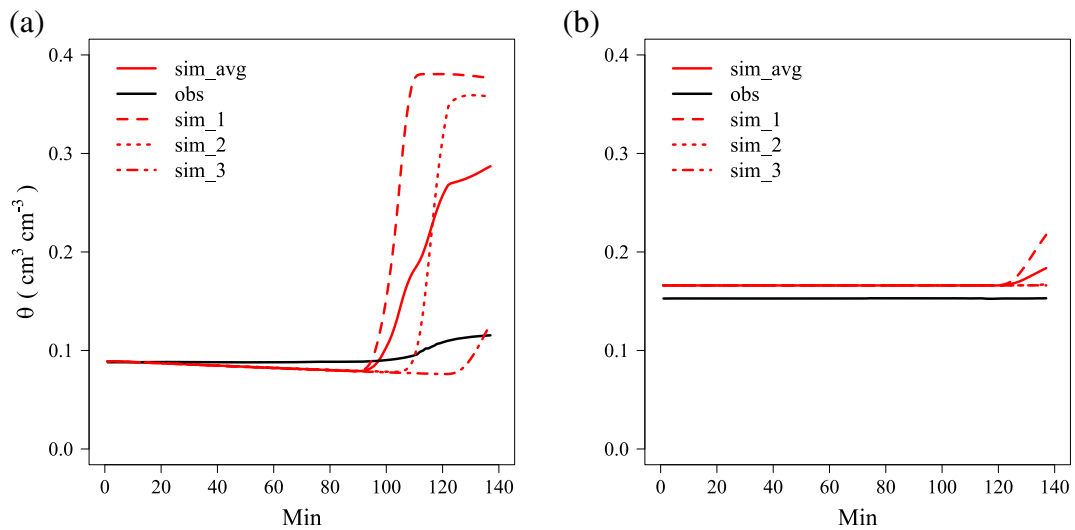


**FIGURE 6** The volumetric water content ( $\theta$ ) of HYDRUS 2D/3D at three observation points for each depth ('sim') versus  $\theta$  from EnviroSCAN ('obs') at 33 cm (a) and 63 cm (b) depth. sim\_1, sim\_2 and sim\_3 are 20, 30, and 40 cm to the right of the infiltration center. sim\_avg is the  $\theta$  average of sim\_1, sim\_2 and sim\_3.

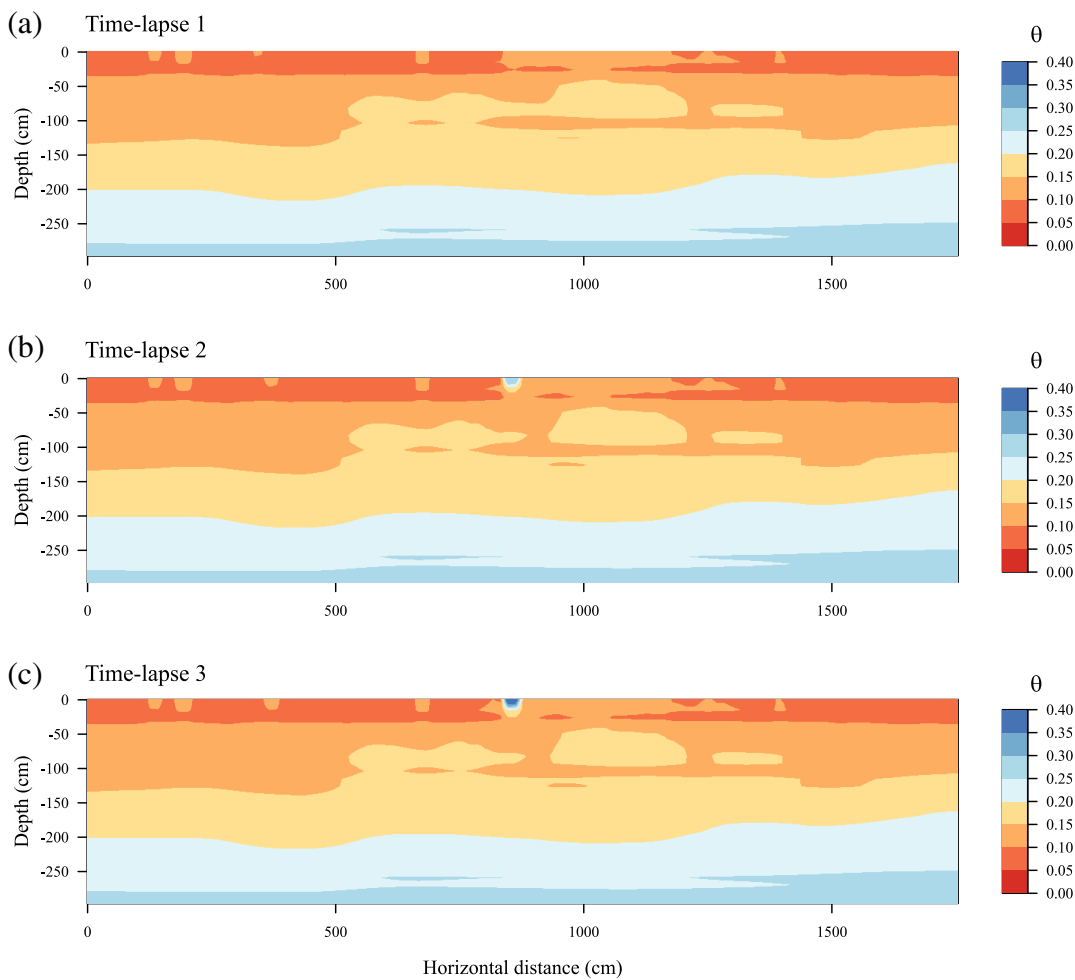


**FIGURE 7** Soil volumetric water content ( $\theta \text{ cm}^3 \text{ cm}^{-3}$ ) estimated by electrical resistivity tomography (ERT) 20 minutes before infiltration (Time-lapse 1, a), 34 (Time-lapse 2, b), and 62 (Time-lapse 3, c) minutes after infiltration. The z-axis represents the soil depth, whereas the x-axis represents the horizontal distance in cm.

**FIGURE 8** In the left (a) volumetric water content difference ( $\Delta\theta$ ,  $\text{cm}^3 \text{cm}^{-3}$ ) between volumetric water content ( $\theta$ ) estimated by portable TDR and electrical resistivity tomography (ERT) in a regular  $10 \times 10$  cm grid (100 points in total). In the center (b), a boxplot of  $\Delta\theta$  for data used in Archie parameter calibration (37 points in total, 30 corresponding to the grid and 7 to EnviroSCAN). In the right (c), a boxplot of  $\Delta\theta$  for independent verification of previous Archie calibration with data between 40 and 100 cm depth (70 data pairs). The red dot in the boxplot is the mean ( $0.009$  or  $-0.019 \text{ cm}^3 \text{cm}^{-3}$ ), the first ( $0.000$  or  $-0.024 \text{ cm}^3 \text{cm}^{-3}$ ), and the third ( $0.022$  or  $-0.013 \text{ cm}^3 \text{cm}^{-3}$ ) quantile are also represented. The negative sign means that ERT overestimates the observed  $\theta$  of portable TDR.

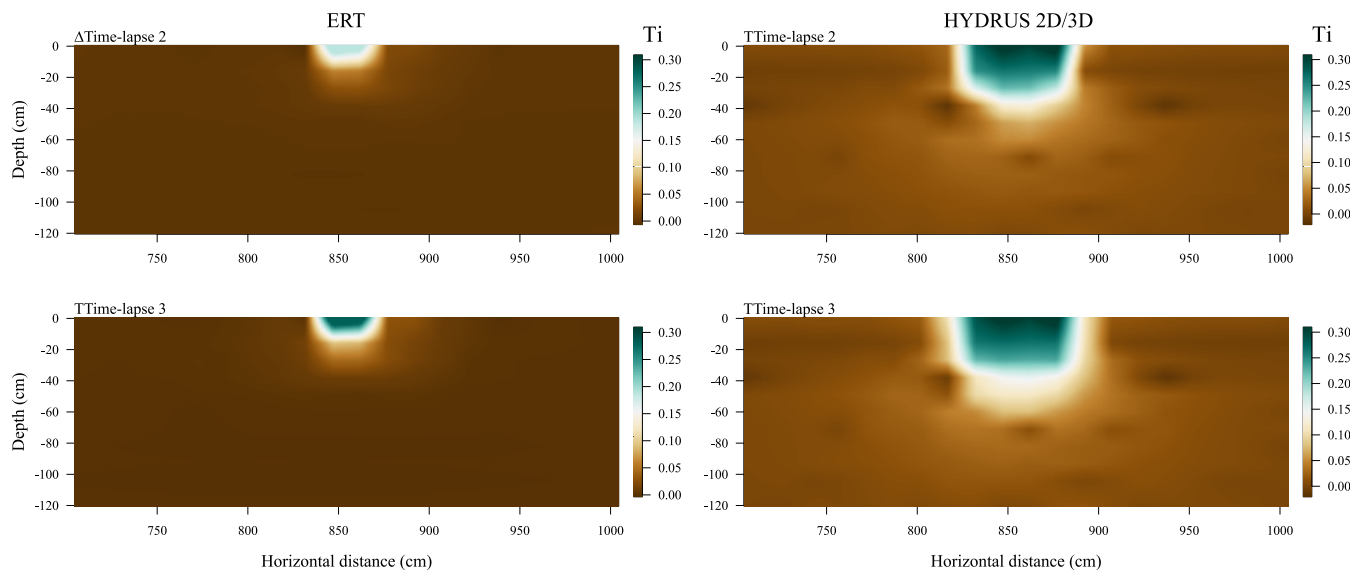
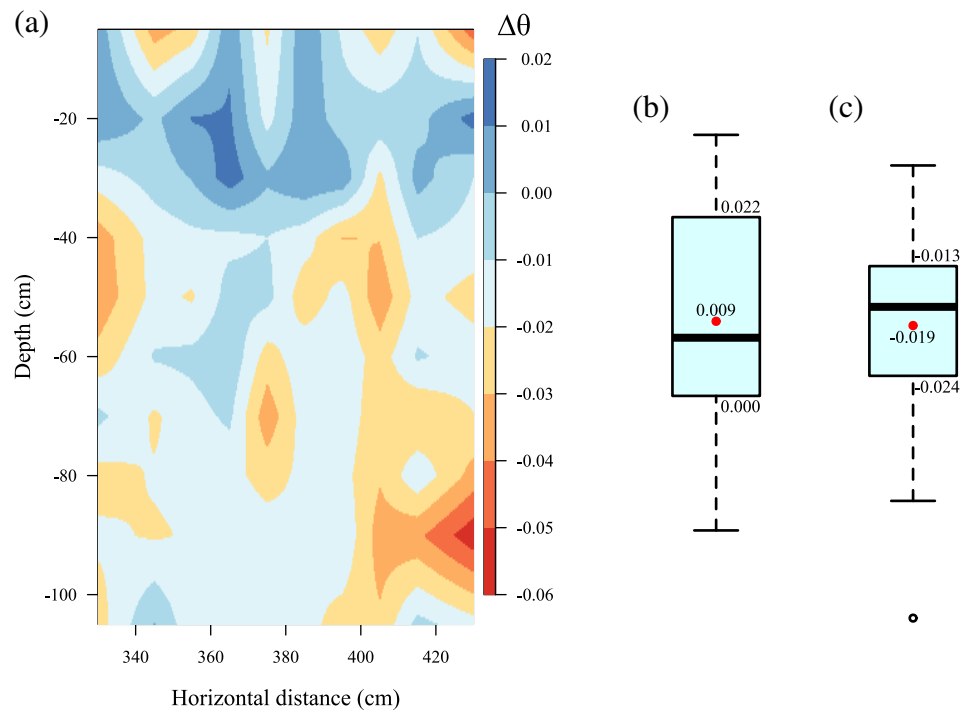


**FIGURE 9** Comparison of change in volumetric water content ( $\Delta\theta$ ,  $\text{cm}^3 \text{cm}^{-3}$ ) between electrical resistivity tomography (ERT) and HYDRUS 2D/3D.  $\Delta\text{Time} - \text{lapse } 2,3$  means the subtraction of  $\theta$  in Time-lapse 2,3 (34 and 62 min after infiltration) against  $\theta$  in Time-lapse 1 (20 min before infiltration or initial time for HYDRUS 2D/3D). The y-axis represents soil depth, and the x-axis represents the horizontal distance in cm. Note that the image is a zoom of Figure 7.

## 4 | DISCUSSION

### 4.1 | HYDRUS 1D and HYDRUS 2D/3D simulations

One of the critical steps in this research is calibrating the soil hydraulic parameters obtained at laboratory conditions for HYDRUS 1D. As shown in Figure 2, ERT and HYDRUS 2D/3D water content

estimation depends on this optimization. Any error performed during calibration will propagate to ERT and HYDRUS 2D/3D  $\theta$  estimation. Thus, we used advanced global sensitivity methods (Figure 4) to determine highly influential parameters before calibration. Sensitivity analysis has been mentioned since decades ago as a valuable tool for hydrological modelling during its development, calibration, and further model verification (McCuen, 1973). This method has been successfully applied with HYDRUS in previous research (Brunetti et al., 2018;

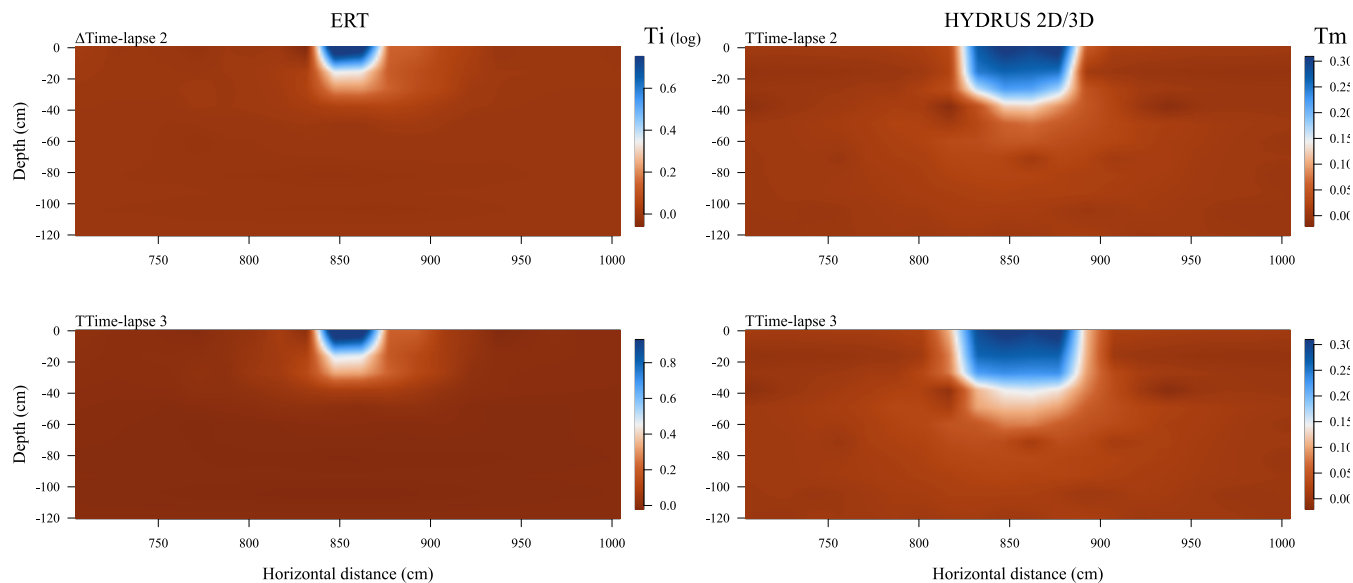


**FIGURE 10** Comparison of the qualitative change of inverted resistivity data ( $\Delta\rho_{(\log)}, \Omega \cdot m$ ) obtained by electrical resistivity tomography (ERT) and the change of  $\theta$  by HYDRUS 2D/3D.  $\Delta$ Time – lapse 2,3 means the subtraction of Time-lapse 2,3 (34 and 62 min after infiltration) against Time-lapse 1 (20 min before infiltration or initial time for HYDRUS 2D/3D). In ERT is computed the change of resistivity ( $\Delta\rho_{(\log)}, \Omega \cdot m$ ) between Time-lapse in logarithm (base 10) and then multiply by  $-1$  to have a comparable colour scale with HYDRUS 2D/3D. The HYDRUS 2D/3D plot depicted the change of volumetric water content ( $\Delta\theta$ ) between Time-lapse. The y-axis represents soil depth, and the x-axis represents the horizontal distance in cm.

Faúndez Urbina et al., 2022; Peddinti et al., 2018). Morris's screening sensitivity analysis method produces five highly influential parameters for calibrating HYDRUS 1D with PEST (Figure 4). The calibration outcomes in Table 2 depict narrow 95% confidence limits, indicating good inverse estimation (Faúndez Urbina et al., 2021). The RMSE obtained in this study for HYDRUS 1D ranged from 0.021 to 0.034  $\text{cm}^3 \text{cm}^{-3}$  after calibrating soil hydraulic parameters. This RMSE is generally like previous studies with HYDRUS after calibrating soil hydraulic parameters (Chakraborty et al., 2022; González et al., 2015; Moghbel et al., 2022; Phogat et al., 2013; Ventrella et al., 2019). Additionally, as in previous studies, the Nash-Sutcliffe coefficient obtained in this research after calibration ranged from 0.11 to 0.77 (Phogat et al., 2013; Ventrella et al., 2019).

Even though the calibration results seem good and comparable with previous research, we observed that the  $n$  parameter of the third material ( $n_3$ ) was modified strongly after calibration (see Tables 1 and 2 for  $n_3$ ). This issue promotes the second field campaign for a detailed soil hydraulic characteristic curve mentioned in Section 2.4.1. However, the value obtained in laboratory conditions (Table 1) was again not close to the one after calibration (Table 2). These results motivate us to try more calibrations, including more parameters (highly influential and influential parameters as defined in Lammoglia et al. (2017)) for calibration than those presented in this research (results not shown). These different calibrations aimed to see if the  $n_3$  parameter compensated for other uncalibrated parameters. This extra calibration substantially improves the RMSE and NSE regarding the ones presented in Figure 5, but with the cost of  $n_3$  even higher than the one

presented in Table 2; therefore, those calibrations were discarded. Thus, we faced whether to trust laboratory-obtained parameters as a baseline for parameter  $n_3$  or to trust in-situ  $\theta$  data obtained by EnviroSCAN used to calibrate  $n_3$ . EnviroSCAN data could have been influenced by a local condition, such as 'soil shrimps' that live at the study site and could form macropores in the soil which are common in forest ecosystems (Luo et al., 2019). This air around the tube can explain why  $n_3$  increases after calibration regarding laboratory measurements. Additionally, these macropores might explain why EnviroSCAN data had water content peaks at 97 and 163 cm depth (Figure 5d,e) that HYDRUS 1D did not simulate. Finally, we chose to calibrate only the highly influential parameters, looking for a balance between good statistics (RMSE and Nash) and realistic parameter estimation as close as possible to laboratory measurements because no further information about macropores was available.

The parameter  $n_3$  corresponds to the third soil material covering 12 to 38 cm of soil, which means the place where the infiltration front was observed (Figures 9 and 10). Figure 5a shows that the Nash-Sutcliffe coefficient and RMSE were not as good as other depths. We hypothesize that the uncertainty on parameter  $n_3$  will affect HYDRUS 2D/3D simulations because  $n_3$  is highly influential, producing lower water content peaks over depth. On the other hand, the influence of this uncertainty in ERT should be less because Archie's law does not use this parameter (Equation (2)).

The comparison of the  $\theta$  obtained by forward simulation of HYDRUS 2D/3D against EnviroSCAN data was unsatisfactory for the 33 cm depth but suitable for the 63 cm depth. For 33 cm depth, it

could be argued that the uncertainties about  $n_3$  were propagated to this forward simulation. However, we observed that the position of EnviroSCAN as an observation point in HYDRUS 2D/3D exerts a strong influence. For example, we observe that sim\_1 (Figures 3 and 6), which is 20 cm from the center of the infiltration front to the center of the EnviroSCAN tube, produces a higher peak of water content than sim\_3, which is 40 cm away. From these results, we assumed that part of the infiltrated water did not reach the EnviroSCAN (e.g., subsurface lateral flow (Farzamian et al., 2015b)), producing this discrepancy. This condition was previously observed in a forced infiltration experiment by Looms et al. (2008), where around 50% of water diverts out of the measurement area because of lateral subsurface flow.

## 4.2 | Water content determination by ERT

ERT inversions have significant limitations related to data quality and geophysical interpretation. One primary concern is the effect of subsurface heterogeneity and electrode distribution, which may result in artefacts in the inversion results. Particularly noteworthy is the impact of having two bodies with high resistivity differences, leading to a degeneration of the inverse problem. This situation introduces high uncertainty, rendering the subsurface resistivity distribution with no unique or stable solution, and may produce non-physical or ambiguous outcomes (Dumont et al., 2016; Friedel, 2003). Considering the shallow exploration depth, we discard this issue, especially in a sedimentary environment where soils are contemporarily deposited. Moreover, spatial resolution limitations of the electrodes can hinder the accurate identification of geological structures or anomalies of interest (Fustos et al., 2020; Metwaly et al., 2009). However, in our ERT deployment in Central Chile, we achieved unprecedented spatial resolution for soils, surpassing previous studies that conducted a resolution of 3 meters to locate temporal aquifers on a slope (Fustos et al., 2017). This improved resolution allows us to represent the soil deposit utilizing Archie's approach for a wetting front.

We emphasize the excellent quality of our inverted resistivity/soil moisture inversion achieved through the Archie model using the TDR grid and EnviroSCAN (Figure 3). The calibration results demonstrated high performance with an RMSE of  $0.017 \text{ cm}^3 \text{ cm}^{-3}$  (Figure 8), and the validation RMSE was only slightly higher at  $0.021 \text{ cm}^3 \text{ cm}^{-3}$ . These results surpass the literature's standards, as previous studies by Rieder and Kneisel (2023) reported depth-dependent RMSE values ranging from 0.01 to  $0.02 \text{ cm}^3 \text{ cm}^{-3}$ . In Chen et al. (2019) and Pedinti et al. (2020), an RMSE between ERT and soil water probe ranged from 0.02 to 0.027 (depth dependent) and  $0.03 \text{ cm}^3 \text{ cm}^{-3}$ , respectively. Moreover, the Archie law parameters obtained through calibration and field conditions (as presented in Table 1) are consistent with those found in previous research conducted by Nijland et al. (2010) and Rieder and Kneisel (2023). This alignment with prior studies adds confidence to the validity of our ERT-based  $\theta$  determination and reinforces the reliability of the results obtained in this study.

The water content data obtained by ERT before and two times after infiltration (also shown in Figure 7) align with the expected behaviour of an infiltration process into the soil. This agreement provides further support for the reliability and accuracy of ERT in determining soil water content dynamics. These promising results highlight the feasibility of conducting future studies in Central Chile once the model is calibrated correctly.

## 4.3 | Comparison of HYDRUS 2D/3D and ERT

Figures 9 and 10 compare HYDRUS 2D/3D and ERT. HYDRUS 2D/3D wetting front is observed to be deeper than ERT's. It is seen from Figures 9 and 10 that roughly the wetting front of ERT is 40 cm and HYDRUS 2D/3D 60 cm (white colours also indicate differences). The previous aligns with  $\theta$  estimated by EnviroSCAN, where no  $\theta$  change was observed at 63 cm depth (Figure 6b). This outcome is significant because ERT and HYDRUS 2D/3D independently determine  $\theta$ . Unfortunately, no  $\theta$  sensors between 33 and 63 cm depth were available with EnviroSCAN. Therefore, we cannot conclude which method was closer to the baseline. The mismatch between HYDRUS 2D/3D and ERT observed in this research has been reported in previous studies. Farzamian et al. (2015a) concluded that the mismatch between HYDRUS 2D and ERT was due to soil heterogeneity not included in HYDRUS. Hardie et al., 2018 observed different wetting patterns between HYDRUS 2D/3D and ERT and mentioned that the cause was preferential flow not included in the model. Ganz et al. (2014) mentioned that ERT and HYDRUS 2D/3D comparison was close when hysteresis was included in the model.

An underestimation of the wetting front from ERT regarding the HYDRUS 2D/3D one could be expected because we used 30 cm electrode separation, which provides around 15–20 cm squared pixels equal to the one used in Farzamian et al. (2015b) for a water injection test. This pixel size will produce the water content 'diluted' at the wetting front. This antecedent suggests that the electrode separation should be reduced in subsequent studies. Additionally, we could expect some underestimation for applying Archie law, which is observed comparing the ERT wetting front in Figures 9 and 10 and previously reported in Farzamian et al. (2015b). Finally, previous discussions suggest that the wetting front is not at ERT or HYDRUS 2D/3D position but somewhere in between.

## 4.4 | Outlook

From previous discussions, we highlight two challenges for subsequent studies. First, the electrode separation and time acquisition of ERT data should be the subject of future research regarding soil parameter estimation using forced infiltration experiments. To our knowledge, no study has been performed to anticipate a specific electrode separation and time acquisition. Secondly, the soil heterogeneity should be more detailed, especially for HYDRUS 2D/3D model simulations. Previous studies (Hardie et al. (2018); Farzamian et al. (2015a)

and Ganz et al. (2014) mentioned that this condition mainly produced the deviation between HYDRUS and ERT for  $\theta$  comparison.

## 5 | CONCLUSION

Determination of soil water content in forest ecosystems is challenging because of soil vertical and spatial heterogeneity, along with deep rooting systems. This research aims to test two undisturbed methods, ERT and HYDRUS 2D/3D, for obtaining water content in a 2D soil profile until the phreatic table. This study shows that HYDRUS 1D obtained reasonable adjustment with EnviroSCAN water content data with RMSE and Nash-Sutcliffe coefficients ranging from 0.021 to 0.034  $\text{cm}^3 \text{cm}^{-3}$  and 0.11 to 0.77, respectively. On the other hand, the forward simulation of HYDRUS 2D/3D using previously calibrated HYDRUS 1D values was inadequate; however, it follows the trend of EnviroSCAN with near to zero variation of water content at 63 cm depth. Furthermore, this study indicates that water content determination by ERT was satisfactory with RMSE for calibration and verification of 0.017 and 0.021  $\text{cm}^3 \text{cm}^{-3}$ , with underestimation and overestimation of water content over the soil profile. An exciting outcome of this research is using a standard grid for interpolating HYDRUS 2D/3D and ERT data to compare both methods with the possibility of an automated run. HYDRUS 2D/3D and ERT comparisons were not equal, with a shallower wetting front by ERT and a deeper one for HYDRUS. Still, both wetting fronts agree with the wetting depth range estimated by EnviroSCAN. We conclude that both methods are an alternative for water content determination in forest ecosystems, with improvements suggested in the discussion section for the following studies.

### ACKNOWLEDGEMENTS

Carlos Faúndez Urbina thanks Mauricio Galleguillos for purchasing HYDRUS 2D/3D licence and data gathering.

### FUNDING INFORMATION

This research was funded by Agencia Nacional de Investigación y Desarrollo (ANID), Chile, FONDECYT de Iniciación grant number 11230533, and FONDECYT regular grant number 1210932, Center for Climate Resilience Research FONDAP-ANID 1522A000.

### CONFLICT OF INTEREST STATEMENT

The authors declare no conflicts of interest.

### DATA AVAILABILITY STATEMENT

The data that support the findings of this study are available from the corresponding author upon reasonable request.

### ORCID

Carlos A. Faúndez Urbina  <https://orcid.org/0000-0003-4925-5277>

Ivo J. Fustos  <https://orcid.org/0000-0002-3542-5477>

Sebastián Elgueta Palma  <https://orcid.org/0000-0002-5931-5889>

## REFERENCES

- Balocchi, F., Galleguillos, M., Rivera, D., Stehr, A., Arumi, J. L., Pizarro, R., García-Chevesich, P., Iroumé, A., Armesto, J. J., Hervé-Fernández, P., Oyarzún, C., Barría, P., Little, C., Mancilla, G., Yépez, S., Rodríguez, R., White, D. A., Silberstein, R. P., Neary, D. G., & Ramírez de Arellano, P. (2023). Forest hydrology in Chile: Past, present, and future. *Journal of Hydrology*, 616, 128681. <https://doi.org/10.1016/j.jhydrol.2022.128681>
- Beck, H. E., Zimmermann, N. E., McVicar, T. R., Vergopolan, N., Berg, A., & Wood, E. F. (2018). Present and future Köppen-Geiger climate classification maps at 1-km resolution. *Scientific Data*, 5(1), 180214. <https://doi.org/10.1038/sdata.2018.214>
- Beevers, L., Bedinger, M., McClymont, K., & Visser-Quinn, A. (2021). Resilience in complex catchment systems. *Water*, 13(4), 541. <https://doi.org/10.3390/w13040541>
- Besson, A., Cousin, I., Bourennane, H., Nicoulaud, B., Pasquier, C., Richard, G., Dorigny, A., & King, D. (2010). The spatial and temporal organization of soil water at the field scale as described by electrical resistivity measurements. *European Journal of Soil Science*, 61(1), 120–132. <https://doi.org/10.1111/j.1365-2389.2009.01211.x>
- Beyá-Marshall, V., Arcos, E., Seguel, Ó., Galleguillos, M., & Kremer, C. (2022). Optimal irrigation management for avocado (cv. 'Hass') trees by monitoring soil water content and plant water status. *Agricultural Water Management*, 271, 107794. <https://doi.org/10.1016/j.agwat.2022.107794>
- Blume, T., Zehe, E., & Bronstert, A. (2009). Use of soil moisture dynamics and patterns at different spatio-temporal scales for the investigation of subsurface flow processes. *Hydrology and Earth System Sciences*, 13(7), 1215–1234. <https://doi.org/10.5194/HESS-13-1215-2009>
- Blume, T., Zehe, E., Reusser, D. E., Iroumé, A., & Bronstert, A. (2008). Investigation of runoff generation in a pristine, poorly gauged catchment in the Chilean Andes I: A multi-method experimental study. *Hydrological Processes*, 22(18), 3661–3675. <https://doi.org/10.1002/HYP.6971>
- Brunet, P., Clément, R., & Bouvier, C. (2010). Monitoring soil water content and deficit using electrical resistivity tomography (ERT): A case study in the Cevennes area, France. *Journal of Hydrology*, 380(1–2), 146–153. <https://doi.org/10.1016/J.JHYDROL.2009.10.032>
- Brunetti, G., Šimůnek, J., Turco, M., & Piro, P. (2018). On the use of global sensitivity analysis for the numerical analysis of permeable pavements. *Urban Water Journal*, 15(3), 269–275. <https://doi.org/10.1080/1573062X.2018.1439975>
- Campolongo, F., Cariboni, J., & Saltelli, A. (2007). An effective screening design for sensitivity analysis of large models. *Environmental Modelling & Software*, 22(10), 1509–1518. <https://doi.org/10.1016/j.envsoft.2006.10.004>
- Casagrande, E., Recanati, F., Rulli, M. C., Bevacqua, D., & Melia, P. (2021). Water balance partitioning for ecosystem service assessment. A case study in the Amazon. *Ecological Indicators*, 121, 107155. <https://doi.org/10.1016/j.ecolind.2020.107155>
- Chakraborty, P., Singh, J., Singh, N., & Kumar, S. (2022). Assessing the influence of cover crop on soil water dynamics using soil moisture measurements and hydru-1D simulations. *Soil Science Society of America Journal*, 86(6), 1538–1552. <https://doi.org/10.1002/saj2.20477>
- Chen, B., Garré, S., Liu, H., Yan, C., Liu, E., Gong, D., & Mei, X. (2019). Two-dimensional monitoring of soil water content in fields with plastic mulching using electrical resistivity tomography. *Computers and Electronics in Agriculture*, 159, 84–91. <https://doi.org/10.1016/j.compag.2019.02.028>
- CIREN. (1997). Estudio Agrológico, Descripción de suelos, materiales y símbolos: VII Región (Publicación N°117). CIREN (Centro de Información de Recursos Naturales. Publicación CIREN N°117).
- Doherty, J. (2015). Calibration and uncertainty analysis for complex environmental models. *Watermark Numerical Computing*.

- Dumont, G., Pilawski, T., Dzaomuhó-Lenieregúe, P., Hiligsmann, S., Delvigne, F., Thonart, P., Robert, T., Nguyen, F., & Hermans, T. (2016). Gravimetric water distribution assessment from geoelectrical methods (ERT and EMI) in municipal solid waste landfill. *Waste Management*, 55, 129–140. <https://doi.org/10.1016/j.wasman.2016.02.013>
- Eitzinger, J., Trnka, M., Hósch, J., Žalud, Z., & Dubrovský, M. (2004). Comparison of CERES, WOFOST and SWAP models in simulating soil water content during growing season under different soil conditions. *Ecological Modelling*, 171(3), 223–246. <https://doi.org/10.1016/j.ecolmodel.2003.08.012>
- Fan, J., Scheuermann, A., Guyot, A., Baumgartl, T., & Lockington, D. A. (2015). Quantifying spatiotemporal dynamics of root-zone soil water in a mixed forest on subtropical coastal sand dune using surface ERT and spatial TDR. *Journal of Hydrology*, 523, 475–488. <https://doi.org/10.1016/j.jhydrol.2015.01.064>
- Farzámian, M., Monteiro Santos, F. A., & Khalil, M. A. (2015a). Application of EM38 and ERT methods in estimation of saturated hydraulic conductivity in unsaturated soil. *Journal of Applied Geophysics*, 112, 175–189. <https://doi.org/10.1016/j.jappgeo.2014.11.016>
- Farzámian, M., Monteiro Santos, F. A., & Khalil, M. A. (2015b). Estimation of unsaturated hydraulic parameters in sandstone using electrical resistivity tomography under a water injection test. *Journal of Applied Geophysics*, 121, 71–83. <https://doi.org/10.1016/j.jappgeo.2015.07.014>
- Fáth, J., Kunz, J., & Kneisel, C. (2022). Monitoring spatiotemporal soil moisture changes in the subsurface of forest sites using electrical resistivity tomography (ERT). *Journal of Forestry Research*, 33(5), 1649–1662.
- Faúndez Urbina, C.A., Kremer, C., Garrido, M., Galleguillos, M., Aponte H, Honorio de Miranda, J., & Seguel, O. (2022). Testing the model efficiency of HYDRUS 2D/3D under desert conditions for water content and pore electrical conductivity: A case study in an olive orchard. *Journal of Soil Science and Plant Nutrition*, 22(2), 1859–1872. <https://doi.org/10.1007/s42729-022-00777-0>
- Faúndez Urbina, C. A., van Dam, J., Tang, D., Gooren, H., & Ritsema, C. (2021). Estimating macropore parameters for HYDRUS using a meta-model. *European Journal of Soil Science*, 72(5), 2006–2019. <https://doi.org/10.1111/ejss.13103>
- Faúndez Urbina, C. A., van den Berg, F., van Dam, J. C., Tang, D. W. S., & Ritsema, C. J. (2020). Parameter sensitivity of SWAP-PEARL models for pesticide leaching in macroporous soils. *Vadose Zone Journal*, 19(1), e20075. <https://doi.org/10.1002/vzj2.20075>
- Ferré, P. A., Knight, J. H., Rudolph, D. L., & Kachanoski, R. G. (1998). The sample areas of conventional and alternative time domain reflectometry probes. *Water Resources Research*, 34(11), 2971–2979. <https://doi.org/10.1029/98WR02093>
- Friedel, S. (2003). Resolution, stability and efficiency of resistivity tomography estimated from a generalized inverse approach. *Geophysical Journal International*, 153, 305–316. <https://doi.org/10.1046/j.1365-246x.2003.01890.x>
- Fustos, I., Moreno-Yaeger, P., Vasquez, D., Morales, B., Silva, A., & Ramirez, E. (2020). Evaluation of rainfall-induced landslides triggering using a multidisciplinary approach. *Universitas Scientiarum*, 25(2), 277–298. <https://doi.org/10.11144/javeriana.sc25-2.eorl>
- Fustos, I., Remy, D., Abarca-Del-Río, R., & Muñoz, A. (2017). Slow movements observed with in situ and remote-sensing techniques in the central zone of Chile. *International Journal of Remote Sensing*, 38(24), 7514–7530. <https://doi.org/10.1080/01431161.2017.1317944>
- Galleguillos, M., Jacob, F., Prévot, L., Faúndez, C., & Bsaibes, A. (2017). Estimation of actual evapotranspiration over a rainfed vineyard using a 1-D water transfer model: A case study within a Mediterranean watershed. *Agricultural and Water Management*, 184, 67–76. <https://doi.org/10.1016/j.agwat.2017.01.006>
- Ganz, C., Bachmann, J., Noell, U., Duijnsveld, W. H. M., & Lamparter, A. (2014). Hydraulic modeling and in situ electrical resistivity tomography to analyze ponded infiltration into a water repellent sand. *Vadose Zone Journal*, 13(1), 1–14. <https://doi.org/10.2136/vzj2013.04.0074>
- Garré, S., Hyndman, D., Mary, B., & Werban, U. (2021). Geophysics conquering new territories: The rise of “agrogeophysics.”. *Vadose Zone Journal*, 20(4), e20115. <https://doi.org/10.1002/vzj2.20115>
- Garré, S., Javaux, M., Vanderborcht, J., Pagès, L., & Vereecken, H. (2011). Three-dimensional electrical resistivity tomography to monitor root zone water dynamics. *Vadose Zone Journal*, 10(1), 412–424. <https://doi.org/10.2136/vzj2010.0079>
- Glover, P. W. J. (2016). Archie's law – A reappraisal. *Solid Earth*, 7(4), 1157–1169. <https://doi.org/10.5194/se-7-1157-2016>
- González, M. G., Ramos, T. B., Carlesso, R., Paredes, P., Petry, M. T., Martins, J. D., Aires, N. P., & Pereira, L. S. (2015). Modelling soil water dynamics of full and deficit drip irrigated maize cultivated under a rain shelter. *Biosystems Engineering*, 132, 1–18. <https://doi.org/10.1016/j.biosystemseng.2015.02.001>
- Grinevskii, S. O. (2011). Modeling root water uptake when calculating unsaturated flow in the vadose zone and groundwater recharge. *Moscow University Geology Bulletin*, 66(3), 189–201. <https://doi.org/10.3103/S0145875211030057>
- Han, Q., Zeng, Y., Zhang, L., Wang, C., Prikaziuj, E., Niu, Z., & Su, B. (2023). Global long term daily 1 km surface soil moisture dataset with physics informed machine learning. *Scientific Data*, 10, 101. <https://doi.org/10.1038/s41597-023-02011-7>
- Hardie, M., Ridges, J., Swarts, N., & Close, D. (2018). Drip irrigation wetting patterns and nitrate distribution: Comparison between electrical resistivity (ERI), dye tracer, and 2D soil–water modelling approaches. *Irrigation Science*, 36(2), 97–110. <https://doi.org/10.1007/s00271-017-0567-3>
- Jia, Y., Gao, W., Sun, X., & Feng, Y. (2023). Simulation of soil water and salt balance in three water-saving irrigation technologies with HYDRUS-2D. *Agronomy*, 13(1), 1–17. <https://doi.org/10.3390/agronomy13010164>
- Karandish, F., & Šimůnek, J. (2019). A comparison of the HYDRUS (2D/3D) and SALTMED models to investigate the influence of various water-saving irrigation strategies on the maize water footprint. *Agricultural Water Management*, 213, 809–820. <https://doi.org/10.1016/j.agwat.2018.11.023>
- Krzeminska, D., Bloem, E., Starkloff, T., & Stolte, J. (2022). Combining FDR and ERT for monitoring soil moisture and temperature patterns in undulating terrain in South-Eastern Norway. *Catena*, 212, 106100. <https://doi.org/10.1016/j.catena.2022.106100>
- Lammoglia, S. K., Makowski, D., Moeys, J., Justes, E., Barriuso, E., & Mamy, L. (2017). Sensitivity analysis of the STICS-MACRO model to identify cropping practices reducing pesticides losses. *Science of the Total Environment*, 580, 117–129. <https://doi.org/10.1016/j.scitotenv.2016.10.010>
- Loke, M. H. (2001). Tutorial: 2-D and 3-D electrical imaging surveys.
- Looms, M. C., Binley, A., Jensen, K. H., Nielsen, L., & Hansen, T. M. (2008). Identifying unsaturated hydraulic parameters using an integrated data fusion approach on cross-borehole geophysical data. *Vadose Zone Journal*, 7(1), 238–248. <https://doi.org/10.2136/vzj2007.0087>
- Luo, Z., Niu, J., Xie, B., Zhang, L., Chen, X., Berndtsson, R., Du, J., Ao, J., Yang, L., & Zhu, S. (2019). Influence of root distribution on preferential flow in deciduous and coniferous Forest soils. *Forests*, 10(11), 986. <https://doi.org/10.3390/f10110986>
- McCuen, R. H. (1973). The role of sensitivity analysis in hydrologic modeling. *Journal of Hydrology*, 18(1), 37–53. [https://doi.org/10.1016/0022-1694\(73\)90024-3](https://doi.org/10.1016/0022-1694(73)90024-3)
- Melo, D. C. D., Anache, J. A. A., Borges, V. P., Miralles, D. G., Martens, B., Fisher, J. B., Nóbrega, R. L. B., Moreno, A., Cabral, O. M. R., Rodrigues, T. R., Bezerra, B., Silva, C. M. S., Neto, A. A. M., Moura, M. S. B., Marques, T. V., Campos, S., Nogueira, J. S., Rosolem, R., Souza, R. M. S., ... Wendland, E. (2021). Are remote sensing evapotranspiration models reliable across south American ecoregions? *Water Resources Research*, 57(11), e2020WR028752. <https://doi.org/10.1029/2020WR028752>

- Metwaly, M., El-Qady, G., Massoud, U., El-Kenawy, A., Matsushima, J., & Al-Arifi, N. (2009). Integrated geoelectrical survey for groundwater and shallow subsurface evaluation: Case study at Siliyin spring, El-Fayoum, Egypt. *International journal of earth sciences*, 99, 1427–1436. <https://doi.org/10.1007/s00531-009-0458-9>
- Moene, A. F., & van Dam, J. C. (2013). *Transport in the atmosphere-vegetation-soil continuum*. Cambridge University Press. <https://doi.org/10.1017/cbo9781139043137>
- Moghbel, F., Mosaedi, A., Aguilar, J., Ghahraman, B., Ansari, H., & Gonçalves, M. C. (2022). Uncertainty analysis of HYDRUS-1D model to simulate soil salinity dynamics under saline irrigation water conditions using Markov chain Monte Carlo algorithm. *Agronomy*, 12(11), 1–21. <https://doi.org/10.3390/agronomy12112793>
- Morris, M. D. (1991). Factorial sampling plans for preliminary computational experiments. *Technometrics*, 33(2), 161–174. <https://doi.org/10.2307/1269043>
- Mualem, Y. (1976). A new model for predicting the hydraulic conductivity of unsaturated porous media. *Water Resources Research*, 12(3), 513–522. <https://doi.org/10.1029/WR012i003p00513>
- Nijland, W., van der Meijde, M., Addink, E. A., & de Jong, S. M. (2010). Detection of soil moisture and vegetation water abstraction in a Mediterranean natural area using electrical resistivity tomography. *Catena*, 81(3), 209–216. <https://doi.org/10.1016/j.catena.2010.03.005>
- Pebesma, E. J., Graler, B., & Heuvelink, G. B. M. (2004). Multivariable geostatistics in S: The gstat package. *Computers & Geosciences*, 30, 683–691.
- Peddinti, S. R., Kambhammettu, B. V. N. P., Lad, R. S., Šimůnek, J., Gade, R. M., & Adinarayana, J. (2020). A macroscopic soil-water transport model to simulate root water uptake in the presence of water and disease stress. *Journal of Hydrology*, 587, 124940. <https://doi.org/10.1016/j.jhydrol.2020.124940>
- Peddinti, S. R., Kambhammettu, B. V. N. P., Ranjan, S., Suradhaniwar, S., Badnakhe, M. R., Adinarayana, J., & Gade, R. M. (2018). Modeling soil-water-disease interactions of flood-irrigated mandarin orange trees: Role of root distribution parameters. *Vadose Zone Journal*, 17(1), 170129. <https://doi.org/10.2136/vzj2017.06.0129>
- Phogat, V., Skewes, M. A., Cox, J. W., Alam, J., Grigson, G., & Šimůnek, J. (2013). Evaluation of water movement and nitrate dynamics in a lysimeter planted with an orange tree. *Agricultural Water Management*, 127, 74–84. <https://doi.org/10.1016/j.agwat.2013.05.017>
- Pizarro, E., Galleguillos, M., Barría, P., & Callejas, R. (2022). Irrigation management or climate change? Which is more important to cope with water shortage in the production of table grape in a Mediterranean context. *Agricultural and Water Management*, 263, 107467. <https://doi.org/10.1016/j.agwat.2022.107467>
- Pujol, G., Iooss, B., Veiga, S., Janon, A., Broto, B., Boumhaout, K., Delage, T., Amri, R., Fruth, J., Gilquin, L., Guillaume, J., Idrissi, M., Gratiot, L., Lemaitre, P., Marrel, A., Meynaoui, A., Nelson, B., Monari, F., Oomen, R., ... Weber, F. (2021). Sensitivity: Global sensitivity analysis of model outputs. R Package Version 1.25.0. <https://CRAN.R-project.org/package=sensitivity>
- Raab, N., Meza, F. J., Franck, N., & Bambach, N. (2015). Empirical stomatal conductance models reveal that the isohydric behavior of an Acacia caven Mediterranean Savannah scales from leaf to ecosystem. *Agricultural and Forest Meteorology*, 213, 203–216. <https://doi.org/10.1016/J.AGRFORMET.2015.06.018>
- Rabbel, I., Bogena, H., Neuwirth, B., & Diekkrüger, B. (2018). Using sap flow data to parameterize the Feddes water stress model for Norway spruce. *Water*, 10, 279. <https://doi.org/10.3390/w10030279>
- Revil, A., & Glover, P. W. J. (1998). Nature of surface electrical conductivity in natural sands, sandstones, and clays. *Geophysical Research Letters*, 25(5), 691–694. <https://doi.org/10.1029/98GL00296>
- Rieder, J. S., & Kneisel, C. (2023). Monitoring spatiotemporal soil moisture variability in the unsaturated zone of a mixed forest using electrical resistivity tomography. *Vadose Zone Journal*, 22(3), e20251. <https://doi.org/10.1002/vzj2.20251>
- Samouëlian, A., Cousin, I., Richard, G., Tabbagh, A., & Bruand, A. (2003). Electrical resistivity imaging for detecting soil cracking at the centimetric scale. *Soil Science Society of America Journal*, 67(5), 1319–1326. <https://doi.org/10.2136/sssaj2003.1319>
- Samouëlian, A., Cousin, I., Tabbagh, A., Bruand, A., & Richard, G. (2005). Electrical resistivity survey in soil science: A review. *Soil and Tillage Research*, 83(2), 173–193. <https://doi.org/10.1016/j.still.2004.10.004>
- Sandoval, M., Dörner, J., Seguel, O., Cuevas, J., & Rivera, D. (2012). Métodos de análisis físicos de suelos. Publicaciones del Departamento de Suelos y Recursos Naturales N°5. Universidad de Concepción. Facultad de Agronomía. Dpto. de Suelos y Recursos Naturales. <https://hdl.handle.net/20.500.14001/59208>
- Schaap, M. G., Leij, F. J., & van Genuchten, M. T. (2001). Rosetta: A computer program for estimating soil hydraulic parameters with hierarchical pedotransfer functions. *Journal of Hydrology*, 251(3), 163–176. [https://doi.org/10.1016/S0022-1694\(01\)00466-8](https://doi.org/10.1016/S0022-1694(01)00466-8)
- Schäfer, C., Fäth, J., Kneisel, C., Baumhauer, R., & Ullmann, T. (2023). Multidimensional hydrological modeling of a forested catchment in a German low mountain range using a modular runoff and water balance model. *Frontiers in Forests and Global Change*, 6, 1186304.
- Schoenberger, P. J., Wysocki, D. A., & Benham, E. C. (2012). Soil Survey Staff, Field Book for Describing and Sampling Soils, version 3.0 | NRCS Soils. NRCS-National Soil Survey Center. [https://www.nrcs.usda.gov/wps/portal/nrcs/detail/soils/ref/?cid=nrcs142p2\\_054184](https://www.nrcs.usda.gov/wps/portal/nrcs/detail/soils/ref/?cid=nrcs142p2_054184)
- Šimůnek, J., van Genuchten, M. T., & Šejna, M. (2016). Recent developments and applications of the HYDRUS computer software packages. *Vadose Zone Journal*, 15(7), 1–25. <https://doi.org/10.2136/vzj2016.04.0033>
- Šimunek, J., van Genuchten, T., & Šejna, M. (2012). HYDRUS: Model Use, Calibration, and Validation. *Transactions of the ASABE*, 55(4), 1263–1276. <https://doi.org/10.13031/2013.42239>
- Skaggs, T. H., Trout, T. J., Šimůnek, J., & Shouse, P. J. (2004). Comparison of HYDRUS-2D simulations of drip irrigation with experimental observations. *Journal of Irrigation and Drainage Engineering*, 130(4), 304–310. [https://doi.org/10.1061/\(ASCE\)0733-9437\(2004\)130:4\(304\)](https://doi.org/10.1061/(ASCE)0733-9437(2004)130:4(304))
- Smith, M., Segeren, A., Santos Pereira, L., Perrier, A., & Allen, R. (1990). Report on the Expert Consultation on Procedures for Revision of FAO Guidelines for Prediction of Crop Water Requirements (FAO, Ed.). FAO. <https://www.fao.org/publications/card/es/c/cb7185en/>
- Smith-Ramírez, C., Grez, A., Galleguillos, M., Cerda, C., Ocampo-Melgar, A., Miranda, M. D., Muñoz, A. A., Rendón-Funes, A., Díaz, I., Cifuentes, C., Alaniz, A., Seguel, O., Ovalle, J., Montenegro, G., Saldes-Cortés, A., Martínez-Harms, M. J., Armesto, J. J., & Vita, A. (2023). Ecosystem services of Chilean sclerophyllous forests and shrublands on the verge of collapse: A review. *Journal of Arid Environments*, 211, 104927. <https://doi.org/10.1016/j.jaridenv.2022.104927>
- Sungmin, O., & Orth, R. (2021). Global soil moisture data derived through machine learning trained with in-situ measurements. *Scientific Data*, 8, 170. <https://doi.org/10.1038/s41597-021-00964-1>
- Tan, S., Wu, B., Yan, N., & Zeng, H. (2018). Satellite-based water consumption dynamics monitoring in an extremely arid area. *Remote Sensing*, 10(9), 1–17. <https://doi.org/10.3390/rs10091399>
- van Genuchten, M. T. (1980). A closed-form equation for predicting the hydraulic conductivity of unsaturated soils. *Soil Science Society of America Journal*, 44(5), 892–898. <https://doi.org/10.2136/sssaj1980.03615995004400050002x>
- van Genuchten, M. T., Leij, F. J., & Yates, S. R. (1991). The RETC code for quantifying the hydraulic functions of unsaturated soils (1.0). EPA Report 600/2-91/065, U.S. Salinity Laboratory, USDA, ARS.



- Ventrella, D., Castellini, M., Di Prima, S., Garofalo, P., & Lassabatère, L. (2019). Assessment of the physically-based Hydrus-1D model for simulating the water fluxes of a Mediterranean cropping system. *Water*, 11(8), 1–19. <https://doi.org/10.3390/w11081657>
- Yang, D., Yang, Y., & Xia, J. (2021). Hydrological cycle and water resources in a changing world: A review. *Geography and Sustainability*, 2(2), 115–122. <https://doi.org/10.1016/J.GEOSUS.2021.05.003>
- Zhang, Y., & Schaap, M. G. (2017). Weighted recalibration of the Rosetta pedotransfer model with improved estimates of hydraulic parameter distributions and summary statistics (Rosetta3). *Journal of Hydrology*, 547, 547–553. <https://doi.org/10.1016/j.jhydrol.2017.01.004>
- Zieher, T., Markart, G., Ottowitz, D., Römer, A., Rutzinger, M., Meißl, G., & Geitner, C. (2017). Water content dynamics at plot scale: Comparison of time-lapse electrical resistivity tomography monitoring and pore pressure modelling. *Journal of Hydrology*, 544, 195–209. <https://doi.org/10.1016/j.jhydrol.2016.11.019>

## SUPPORTING INFORMATION

Additional supporting information can be found online in the Supporting Information section at the end of this article.

**How to cite this article:** Faúndez Urbina, C. A., Alanís, D. C., Ramírez, E., Seguel, O., Fustos, I. J., Donoso, P. D., de Miranda, J. H., Rakonjac, N., Palma, S. E., & Galleguillos, M. (2023). Estimating soil water content in a thorny forest ecosystem by time-lapse electrical resistivity tomography (ERT) and HYDRUS 2D/3D simulations. *Hydrological Processes*, 37(10), e15002. <https://doi.org/10.1002/hyp.15002>